2012

Comparing satellite and ground-based observations of paroxysmal degassing events at Etna volcano, Italy

Céline L. Mandon
Michigan Technological University

COMPARING SATELLITE AND GROUND-BASED OBSERVATIONS OF PAROXYSMAL DEGASSING EVENTS AT ETNA VOLCANO, ITALY

By

Céline L. Mandon

A THESIS

Submitted in partial fulfillment of the requirements for the degree of

MASTER OF SCIENCE

(Geology)

MICHIGAN TECHNOLOGICAL UNIVERSITY

2012

This thesis, “Comparing Satellite and Ground-based Observations of Paroxysmal Degassing Events at Etna Volcano, Italy,” is hereby approved in partial fulfillment of the requirements for the Degree of MASTER OF SCIENCE IN GEOLOGY.

Department of Geological and Mining Engineering and Sciences

Signatures:

Thesis Advisor _____
Dr. Simon A. Carn

Department Chair _____
Dr. Wayne D. Pennington

Date _____

Table of contents

List of figures

List of tables

Acknowledgements

I would like to thank my advisor Simon Carn for his help and mentoring during my research, Giuseppe Salerno from the Istituto Nazionale di Geofisica e Vulcanologia of Catania for his collaboration with the ground-based data, and Séverine Moune and Gregory Waite for being part of my committee. I also would like to thank the INVOGE program and all its members, which permitted me this experience in Michigan Tech, and Elisa Piispa for her help and encouragement.

Abstract

Mount Etna, Italy, is one of the most active volcanoes in the world, and is also regarded as one of the strongest volcanic sources of sulfur dioxide (SO_2) emissions to the atmosphere. Since October 2004, an automated ultraviolet (UV) spectrometer network (FLAME) has provided ground-based SO_2 measurements with high temporal resolution, providing an opportunity to validate satellite SO_2 measurements at Etna. The Ozone Monitoring Instrument (OMI) on the NASA Aura satellite, which makes global daily measurements of trace gases in the atmosphere, was used to compare SO_2 amount released by the volcano during paroxysmal lava-fountaining events from 2004 to present. We present the first comparison between SO_2 emission rates and SO_2 burdens obtained by the OMI transect technique and OMI Normalized Cloud-Mass (NCM) technique and the ground-based FLAME Mini-DOAS measurements. In spite of a good data set from the FLAME network, finding coincident OMI and FLAME measurements proved challenging and only one paroxysmal event provided a good validation for OMI. Another goal of this work was to assess the efficacy of the FLAME network in capturing paroxysmal SO_2 emissions from Etna, given that the FLAME network is only operational during daylight hours and some paroxysms occur at night. OMI measurements are advantageous since SO_2 emissions from nighttime paroxysms can often be quantified on the following day, providing improved constraints on Etna's SO_2 budget.

1. Introduction

Sulfur dioxide (SO_2) is an atmospheric trace gas emitted by natural sources such as volcanic eruptions, oxidation of oceanic dimethyl sulphide (DMS) (Berresheim et al. 1995) and anthropogenic sources from the industry. It is dangerous for human health (Ware et al. 1986; Katsouyanni et al. 1997; Hansell and Oppenheimer 2004) and causes acid rain (Likens and Bormann 1974). The lifetime of SO_2 in the lower troposphere is approximately one day at this latitude, where after which it begins to be deposited or oxidized to sulfate (Stevenson et al. 2003). Sulfate aerosol, which has a long lifetime in the stratosphere, reflects incoming solar radiation, causing the cooling of the atmosphere below it (Charlson et al. 1992).

SO_2 is typically the third most abundant volcanic gas species after H_2O and CO_2, so the amount released into the atmosphere during an eruption can be significant and have impacts on climate and environment on both local and regional scales. Monitoring volcanic SO_2 is also very important for volcanologists as it reflects the activity of a volcano. Indeed, changes in SO_2 emission rates show variations within volcanic systems, and such changes can be precursors of an eruption (Casadevall et al. 1981; Caltabiano et al. 1994; Young et al. 1998; Watson et al. 2000; Sutton et al. 2001).
Ash emissions are often coupled with gas emissions during an eruption, which means that ash might be also emitted in the atmosphere. Ash particles, coupled with sulfate aerosol, are known to be a significant hazard to aviation, as the 2010 Eyjafjallajökull eruption demonstrated, and remote sensing of SO_2 provides an effective means of tracking drifting volcanic clouds.

Remote sensing of atmospheric SO_2 is possible due to the low background concentration of the specie in the atmosphere and its strong absorption features in the ultraviolet (UV) region of the electromagnetic spectrum. The first satellite sensor used to measured volcanic SO_2 emissions was the Total Ozone Mapping Spectrometer (TOMS),

after the observation of the 1982 El Chichon eruption cloud (Krueger 1983). Technology has been recently improved, leading to satellites with better spectral and spatial resolutions, such as the Global Ozone Monitoring Equipment (GOME and GOME-2) and the Scanning Imaging Absorption Spectrometer for Atmospheric Cartography (SCIAMACHY).

The spatial and temporal resolutions of the Ozone Monitoring Instrument (OMI) are the best currently available for space-based measurement of volcanic SO_2 emissions in the UV. OMI is a UV/visible sensor launched in July 2004 on the Earth Observing System Aura satellite by NASA. Validation of its trace gas measurements is critical to ensure high-quality SO_2 data. Validation of SO_2 measurements in volcanic clouds is more difficult than for anthropogenic sources, mostly because volcanic eruptions are unpredictable and plume trajectories can be uncertain, and also because of the heterogeneity within the cloud itself. Although some successful validation has been achieved, (Spinei et al. 2010; Carn and Lopez 2011a), ongoing validation is still required, especially for volcanoes with different eruptive styles.

Validation efforts typically require comparison of satellite data and ground-based remote measurements, derived from instruments such as the correlation spectrometer (COSPEC), used for volcanic SO_2 fluxes measurement since the early 1970s (Newcomb and Millán 1970; Moffat and Millán 1971; Stoiber and Jepsen 1973) or more recently Differential Optical Absorption Spectroscopy (DOAS) SO_2 measurements (Noxon 1975; Platt 1994; Platt and Stutz 2008). Because of the unpredictable and hazardous character of volcanic eruptions, ground-based measurements are not always easy. Furthermore, scientists have to be ready to quickly deploy the equipment in places that may not be easily accessible.

Mount Etna, Italy, is known for its globally significant SO_2 release into the atmosphere (Caltabiano et al. 1994; Allard 1997). As well as continuous passive degassing, explosive eruptions generate plumes with a high content of SO_2. A scanning UV spectrometer network, FLAME (FLux Automatic MEasurements),

permits automatic measurement of SO_2 fluxes with high time resolution (~6 min), with data available since October 2004 (Burton et al. 2004; Salerno et al. 2009a).

The aim of this study is to compare OMI SO_2 data with ground-based data from the FLAME network for some paroxysmal events of Mount Etna, and to improve constraints on Etna's SO_2 emissions by quantification of paroxysmal SO_2 discharge.

2. Geological settings

Mount Etna, located on the eastern coast of Sicily (Italy), is a composite stratovolcano 3330 m-high and 0.5 Ma old (Gillot et al. 1994; Corsaro and Cristofolini 1997; Schiano et al. 2001). It is only 30 kilometers from Catania, the second biggest city in Sicily and although the activity is rarely explosive, particle and ash emissions in the atmosphere regularly lead to the closure of the International Airport Fontanarossa.

2.1 Tectonic and Geology

Mount Etna is surrounded by three different geological units: 1) The Calabro-Peloritan unit to the east, which is part of the Alpine-Appenninic orogenic belt; 2) the northern part of the African plate to the south, called the Hyblean Plateau; 3) and to the west, the Appennine-Maghrebian chain. A major fault trending SSE-NNW, the Tindari-Letojanni-Malta fault, crosses this area (Figure 2.1). This is the most likely source for the strongest earthquakes in the area, while the NE-SW fault system in the Hyblean Plateau is active, but with events with weaker magnitudes (Azzaro R. and Barbano M.S. 2000).

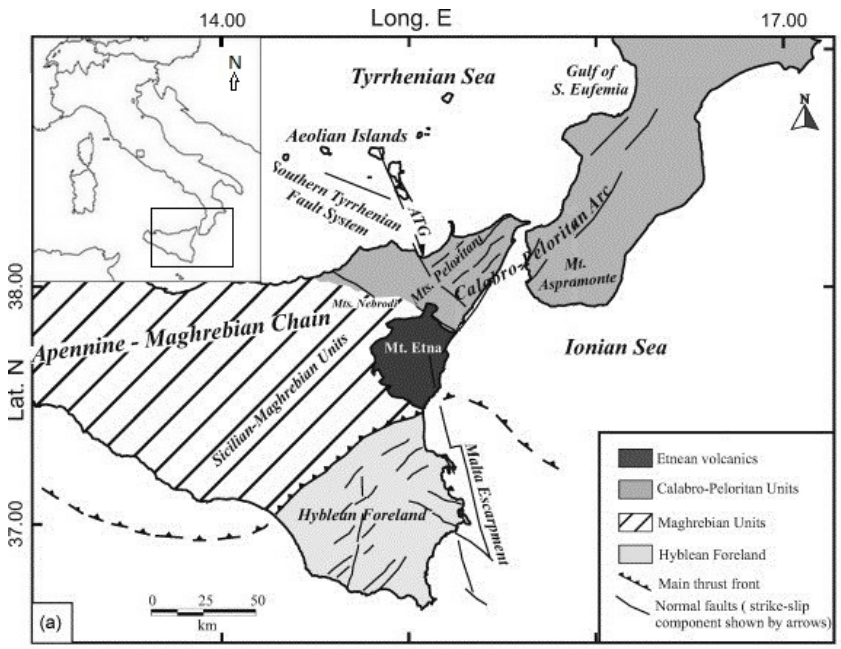

Figure 2.1: Location of Mount Etna and simplified tectonic map of the area. Source: modified from Scarfi et al., 2009.

2.2 Volcanic activity

Mount Etna is the most active volcano in Europe and one of the world's strongest sources of SO_2 emissions (Caltabiano et al. 1994; Allard 1997) derived from continuous degassing of volatile-rich alkaline basalts (Métrich and Clocchiatti 1989; Métrich 1993) at the summit craters: Voragine, Bocca Nuova, South-East and North-East (Figure 2.2). The activity is mainly effusive, with paroxysmal events characterized by strong strombolian explosions that can evolve into pulsating or continuous lava-fountains. However, some sub-plinian and plinian eruptions have been identified in Etna's historic record (Guest et al. 1984; Chester et al. 1987; Coltelli et al. 1995, 1998).

Some of the paroxysmal events that occurred in the last twelve years were studied in order to have a better knowledge of the mechanisms that drive basaltic lava-fountain episodes. There are two physical models to explain this type of activity: 1) the Collapsing Foam (CF) model (Jaupart and Vergniolle 1988, 1989; Vergniolle and Jaupart 1990) that implies the collapse of a foam layer at the top of a shallow magma chamber which causes bubble coalescence and an annular flow that ascend the conduit and feed the lava fountain (previous gas-magma separation); 2) the Rise Speed Dependent (RSD) model (Parfitt 2004) that implies increase of the magma ascent rate, rapid exsolution of volatiles and bubble coalescence during the magma ascent in the conduit (syneruptive degassing).

The 2000 southeast crater lava fountains were the most studied and all the results agree for the foam collapse model with the top of the shallow magma reservoir at 1.5-1.8 km (Allard et al. 2005; Spilliaert et al. 2006; Andronico and Corsaro 2011). More recently, some other lava-fountain events have been explained by this model: the 10 May 2008 eruption (Bonaccorso et al. 2011a), the 11-13 January 2011 eruption, (Calvari et al. 2011), and the 10 April 2011 eruption (Bonaccorso et al. 2011b).

The average flux of SO_2 supplied by passive degassing varies with time depending on the type of activity: 4000-5500 tons per day from 1975 to 1999 (Allard 1997; Bruno et al. 2001), around 1000 tons per day in 2002 (McGonigle et al. 2003) and around 3500 tons per day during the period 2005-2008 (Salerno et al. 2009b). The SO_2 flux can reach 10000-15000 tons per day during vigorous strombolian activity and more than 20000 tons per day during continuous lava fountaining (Allard 1997).

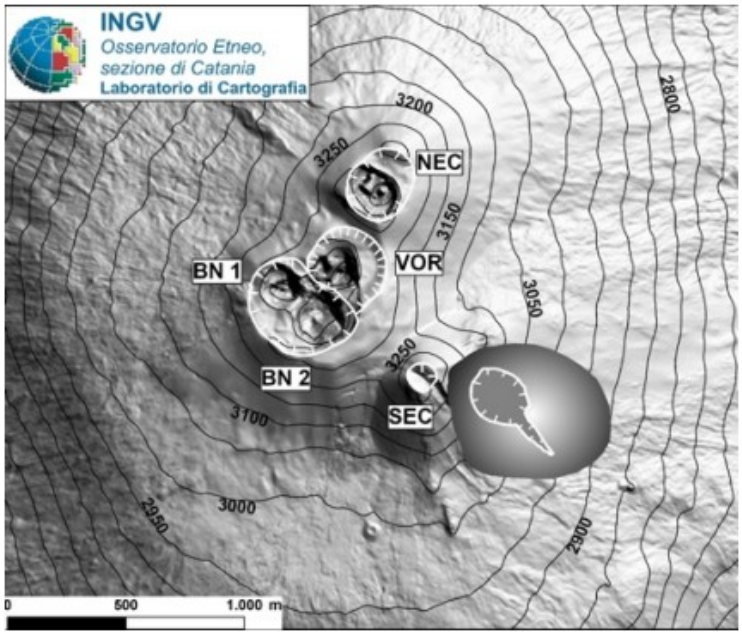

Figure 2.2: Map of Mount Etna with the four summit craters. VOR: Voragine; BN1 and BN2: Bocca Nuova 1 and 2; SEC: South-East Crater; NEC: North-East Crater. The cavity on the east flank of the SEC is the New South-East Crater, formed since the beginning of the 2011 activity. Courtesy of Istituto Nazionale di Geofisica e Vulcanologia, Osservatorio Etneo, Italy.

The origin of the volcanism in this area is still not well understood, mostly because it is located near the subduction of the African plate under the European plate and also above the mantle-plume beneath Sicily. Different theories exist: 1) volcanism related to a backarc marginal basin (Barberi et al. 1974); 2) the rollback motion of the Ionian slab associated with decompression melting of upper mantle material (Gvirtzman and Nur 1999); 3) the rise of a mantle plume from the 670 km discontinuity (Marone et al. 2004; Montelli et al. 2006; Cadoux et al. 2007) or 4) from the deep mantle (Schiano et al. 2001). However, geochemical studies of magma show evidences of a transition from a predominant mantle-plume source to subduction related basalts (Tanguy et al. 1997; Gvirtzman and Nur 1999; Schiano et al. 2001,

Clocchiatti et al. 2004) probably due to the southward migration of the Ionian slab leading to the juxtaposition with the mantle plume beneath Sicily (Schiano et al. 2001). Because the activity of a subduction related volcano can be more explosive than one in a hotspot setting, monitoring and study of Mount Etna's activity is crucial.

2.3 Eruptive history

Mount Etna started to form around 0.5 Ma. Some lahar and tephra deposits give evidence of explosive activity at different periods throughout the volcano's history. The oldest is a tephra deposit estimated to be 150-100 ka old (Condomines et al. 1982; Coltelli et al 2000) followed by evidence of plinian, sub-plinian and strombolian activity until the 15 ka Ellittico caldera formation (Kieffer 1973, 1985; Duncan 1976; Romano and Guest 1979; Guest et al. 1984; Chester et al. 1987; Coltelli 1994, 2000). Some strong eruptions occurred in historic time, including the 122 BC plinian eruption (Coltelli et al. 1998) and the 1669 eruption which killed 15 000 people (Corsaro et al. 1996; Ciuccarelli 2001, 2004; Branca and Del Carlo 2004).

Mount Etna exhibited low activity after the 2001 and 2002-2003 eruptions until 2006. Table 2.1 is a summary of all the paroxysmal events from 2004 to present.

Some big eruptions occurred in 2007 and 2008 after which the activity calmed down. January 2011 was the beginning of a new eruptive cycle, which is still going on. This new eruptive cycle began with the January 12th eruption. Twenty-five paroxysms had occurred since that time, with the last one on April 24th, 2012. The episodes lasted from ~1h30 to ~14h30 and were separated by quiescent intervals ranging from 5 days to 58 days. The paroxysms are characterized by strong strombolian activity and lava fountains.

Table 2.1

Paroxysmal events at Mount Etna from 2004 to present. SEC: South-East crater. Sources: Istituto Nazionale di Geofisica e Vulcanologia (http://www.ct.ingv.it/), Smithsonian and USGS (http://www.volcano.si.edu/world/volcano.cfm?vnum=0101-06=&volpage=weekly). The SO_2 mass emitted was estimated using the Normalized Cloud-Mass technique from the OMIplot software.

Date	Onset time	Duration	Area of activity	Description of activity	Lava flow length	Plume height & Ash erupted	SO2 mass emitted (t)
07/09/04	10:30	1 day	Radial fissure eruption Base of SEC	Effusive eruption	2.5 km $4 * 10^7$ m^3		
16/12/05			Central vent eruption Bocca Nuova	Explosive eruption strombolian activity, ash plume			
22/12/05			Central vent eruption Bocca Nuova	Explosive eruption strombolian activity, ash plume drifted E			
Eruption 14/07 to 14/12/06				Total volume produced : $1.8 \pm 0.3 * 10^7$ m^3			
14/07/06	23:30	10 days	Radial fissure eruption E flank of SEC	Explosive eruption strombolian activity, small ash falls, lava flow	3 km		
31/08/06		16 days	Central vent eruption SEC	Explosive eruption strombolian activity, lava flows, lapilli and bombs, ash plume on 10/09	3 km		
22/09/06	afternoon	5 days	Central vent eruption SEC	Explosive eruption strombolian activity, lava flows			
03/10/06	Late afternoon	3 days	Central vent eruption SEC	Explosive eruption strombolian activity, lava flows			
10/10/06	Evening	1 day	Central vent eruption SEC	Explosive eruption strombolian activity, lava flows	2 km		

Table 2.1, continued

Date	Onset time	Duration	Area of activity	Description of activity	Lava flow length	Plume height & Ash erupted	SO2 mass emitted (t)
20/10/06	06:00	~ 14 hours	Central vent eruption SEC	Explosive eruption strombolian activity, lava flows	< 1 km		
23/10/06	07:00	10h50	Central vent eruption SEC	Explosive eruption strombolian activity, pulsating lava fountain, ash plume at 17:00 drifted ESE	2.5 km		
05/11/06	20:04	~ 9 hours	Central vent eruption SEC	Explosive eruption strombolian activity, lava flows, ash plume			
16/11/06	05:07	10h30	Central vent eruption SEC Radial fissure eruption SSE and SE flank of SEC	Explosive eruption strombolian activity, lava flow, ash plume drifted ENE then NE, rock falls and avalanches	3 km	4 km $7*10^6$ kg	1450
21/11/06	12:00	9h	Central vent eruption SEC Radial fissure eruption SSE and SE flank of SEC	Explosive eruption strombolian activity, lava fountain 300m high at 19:00, ash plume at 15:00, lava flow		4.8 km 10^8 kg	7810
24/11/06	02:19	13h10	Central vent eruption SEC Radial fissure eruption SSE flank of SEC	Explosive eruption strombolian activity, ash plume drifted SE, lava flows		5.3 km 10^8 kg	
30/11/06	16:00	7h	Central vent eruption SEC	Explosive eruption strombolian activity, lava fountain, ash plume, lava flow	4.7 km		
11/04/07	03:00	5h	Central vent eruption SEC	Explosive eruption strombolian activity, lava fountain, ash plume drifted E, 2 lava flows	3 km and < 1 km	5 km	5480

Table 2.1, continued

Date	Onset time	Duration	Area of activity	Description of activity	Lava flow length	Plume height & Ash erupted	SO2 mass emitted (t)
29/04/07	15:00	9h	Central vent eruption SEC	Explosive eruption strombolian activity, lava fountain, ash plume, lava flows		6 km	3860
04/09/07	16:00	13h	Central vent eruption SEC	Explosive eruption strombolian activity, continuous lava fountain 400-600m high, lava flows, ash plume drifted E	4.6 km	4.2 km 3.9-4.9*10^5 m^3	12120
23/11/07	20:20	8h	Central vent eruption SEC and Bocca Nuova	Explosive eruption strombolian activity, continuous lava fountain 600m high, lava flows, ash plume drifted NE	4.2 km	6.5 km	14730
10/05/08	14:00	4h	Central vent eruption SEC	Explosive eruption strombolian activity, ash plume drifted N, lava flows	6.4 km 4.5*10^6 m^3	6.4 km	18300
13/05/08	11:15	6h45	Radial fissure eruption E base of NEC, E flank and base of SEC	Explosive eruption strombolian activity, ash plume drifted NNE, continuous lava fountain 100-150 m high for few hours, lava flows	6 km	4.6-5.3 km	26500
14/05/08			Radial fissure eruption E base of NEC, E flank and base of SEC	Explosive eruption strombolian activity, ash plume drifted NE then S, lava fountain 100 m high, lava flows	5 km	4.5 km	1970
15/05/08			Radial fissure eruption E flank of SEC	Explosive eruption strombolian activity, ash plume drifted SE from 02:50 to 14:17, lava flows	6 km		

Table 2.1, continued

Date	Onset time	Duration	Area of activity	Description of activity	Lava flow length	Plume height & Ash erupted	SO2 mass emitted (t)
16/05/08			Radial fissure eruption E base of NEC, E flank and base of SEC	Explosive eruption strombolian activity, ash plume after 14:06, lava fountain in the morning, lava flows			
17/05/08			Radial fissure eruption E base of NEC, E flank and base of SEC	Explosive eruption strombolian activity, lava flows, ash plume drifted N		max 4 km	
11/07/08	morning	1 day	Radial fissure eruption E flank of SEC	Explosive eruption strombolian activity, lava flow			
25/08/10	15:09	20 min	Central vent eruption Bocca Nuova	Explosive eruption strombolian activity, ash plume drifted E		4.3 km	
12/01/11	21:10	3h40	Radial fissure eruption E flank of SEC	Explosive eruption strombolian activity, lava flows, ash plume drifted SSW, continuous lava-fountain 800 m high	4.3 km	7.3 km	
18/02/11	04:30	8h50	Radial fissure eruption E flank of SEC	Explosive eruption strombolian activity, lava flow, ash emission, pulsating lava fountain		8 km	2600
10/04/11	10:00	6h	Radial fissure eruption E flank of SEC	Explosive eruption strombolian activity, lava fountain 300 m high, gas and ash plume drifted SE, lava flows	2.5 km	5.3 km	1540
12/05/11	03:20	2h50	Radial fissure eruption E flank of SEC	Explosive eruption strombolian activity, lava fountain 300 m high, ash plume drifted SSE, lava flow		5.3 - 6.3 km	

Table 2.1, continued

Date	Onset time	Duration	Area of activity	Description of activity	Lava flow length	Plume height & Ash erupted	SO2 mass emitted (t)
09/07/11	13:15	4h25	Radial fissure eruption E flank of SEC	Explosive eruption strombolian activity, lava flow, continuous lava fountain, ash plume drifted SSE		6.8 km	1750
19/07/11	02:00	3h	Radial fissure eruption E flank of SEC	Explosive eruption strombolian activity, lava flows, lava fountain 250 m high, ash and gas plume drifted E		5 km	
25/07/11	04:00	4h	Radial fissure eruption E flank of SEC	Explosive eruption strombolian activity, lava flows, pulsating lava fountain 350 m high, ash and gas plume drifted E		7 km	4070
30/07/11	10:00	14h30	Radial fissure eruption E flank of SEC	Explosive eruption strombolian activity, lava flows, continuous lava fountain 450-500 m high, ash and gas plume drifted E	3 km	5.7 km	7230
05/08/11	22:30	3h45	Central vent eruption New SEC Radial fissure E flank of the old SEC	Explosive eruption strombolian activity, lava flows, lava fountain 500m high, ash plume drifted SE		10.7 km	2700
12/08/11	09:00	4h	Central vent eruption New SEC	Explosive eruption strombolian activity, pulsating lava fountain 100 m high, lava flows, ash plume		3.7 km	3370
20/08/11	04:55	5h	Central vent eruption New SEC	Explosive eruption strombolian activity, ash and gas plume drifted SW, continuous lava fountain, lava flows, avalanches		9 km	2990

Table 2.1, continued

Date	Onset time	Duration	Area of activity	Description of activity	Lava flow length	Plume height & Ash erupted	SO2 mass emitted (t)
29/08/11	05:46	4h	Central vent eruption New SEC Radial fissure eruption SE flank of SEC	Explosive eruption strombolian activity, lava flow, lava fountain 100 m high, ash plume drifted SSE		9.5 km	3150
08/09/11	08:30	2h15	Central vent eruption New SEC Radial fissure eruption SE and N flank of SEC	Explosive eruption strombolian activity, lava flow, pulsating lava fountain, ash plume		10 km	3210
19/09/11	12:20	2h40	Central vent eruption New SEC	Explosive eruption strombolian activity, lava flows, lava fountain, gas plume drifted NE		7.5 km	780
28/09/11	19:30	2h40	Central vent eruption New SEC	Explosive eruption strombolian activity, lava flows, continuous lava fountain 800 m high, ash plume drifted SW		10.5 km	3710
08/10/11	13:00	4h45	Central vent eruption New SEC Radial fissure eruption SE and N flank of SEC	Explosive eruption strombolian activity, lava flows, continuous lava fountain, ash and gas plume drifted E			
23/10/11	19:40	3h35	Central vent eruption New SEC Radial fissure eruption SE flank of SEC	Explosive eruption strombolian activity, lava flows, continuous lava fountain 300 m high, ash plume drifted ESE, avalanches		5.5 km	2130
15/11/11	10:20	4h30	Central vent eruption New SEC Radial fissure eruption SE and N flank of SEC	Explosive eruption strombolian activity, lava flows, lava fountain 800 m high, ash drifted SE	< 4 km	10.5 km	4770

Table 2.1, continued

Date	Onset time	Duration	Area of activity	Description of activity	Lava flow length	Plume height & Ash erupted	SO2 mass emitted (t)
05/01/12	03:45	4h15	Central vent eruption New SEC Radial fissure eruption SE and N flank of SEC	Explosive eruption strombolian activity, lava flows, continuous lava fountain 150 m high, ash and gas plume drifted SSW, small lahar, pyroclastic flow and phreatomagmatism	2 km	9 km	6520
09/02/12	00:00	11h	Central vent eruption New SEC	Explosive eruption, strombolian activity, lava flows, continuous lava fountain 500 m high, ash plume drifted W	< 3 km	9.3 km	1110
04/03/12	05:30	5h	Central vent eruption New SEC, Radial fissure eruption SW and N flank of SEC	Explosive eruption strombolian activity, lava flows, continuous lava fountain, ash plume drifted NE, pyroclastic flows, lahar, phreatic explosion	3.5 km	7.5 km	
18/03/12	08:00	3h10	Central vent eruption New SEC, Radial fissure eruption N flank of SEC	Explosive eruption strombolian activity, lava fountain, lava flows, avalanches, ash plume drifted E, lahar, pyroclastic flow, phreatic explosion	4 km	7.5 km	6770
01/04/12	03:30	3h10	Central vent eruption New SEC, Radial fissure eruption SE flank of SEC	Explosive eruption strombolian activity, lava fountain, lava flows, gas and ash plume drifted SE, pyroclastic flows, phreatic explosion	< 4km	10.5 km	8270

Table 2.1, continued

Date	Onset time	Duration	Area of activity	Description of activity	Lava flow length	Plume height & Ash erupted	SO2 mass emitted (t)
12/04/12	14:16	3h45	Central vent eruption New SEC	Explosive eruption strombolian activity, lava fountain, lava flows, gas and ash plume drifted E		6.3 km	
24/04/12	03:10	1h30	Central vent eruption New SEC	Explosive eruption strombolian activity, lava fountain, lava flows, gas and ash plume drifted E		5.5 km	13170

3. OMI

3.1 The Ozone Monitoring Instrument

OMI is a Dutch-Finnish polar-orbiting hyperspectral ultraviolet-visible (270-500 nm) spectrometer launched in July 15, 2004 on the Earth Observing System Aura satellite by the NASA. It provides daily, global contiguous mapping of ozone and trace gases including SO_2, NO_2, BrO, HCOH, and OClO. The two-dimensional charge couple device (CCD) detectors that measure backscattered radiances permit acquisition of spectral and spatial information at the same time. It has a 2600 km swath, spatial resolution of 13×24 km at nadir and a local afternoon equatorial crossing time at 13:45 which make it one of the best satellite sensors for SO_2 measurements launched to date (Levelt et al. 2006).

SO_2 is detected using its well-characterized differential absorption structure in the UV wavelength region, which must be separated from that due to stratospheric ozone in the same region. The OMI channel used to detect SO_2 is UV-2, from 310 nm to 365 nm, with a spectral resolution of 0.45 nm (Levelt et al. 2006). It also provides measurements of gas traces column amounts, aerosol index (AI), UV reflectivity, cloud top pressure and cloud fraction.

Since June 2007, an anomaly has been observed in the OMI data, called the row anomaly, affecting different cross-track scenes. Radiances measured within the row anomaly are not useable for trace gas retrievals, leading to stripes without data in each OMI swath. This row anomaly data gap prevented measurement of the Etna plume for some eruptions in 2011 and 2012, precluding calculation of the SO_2 mass in the volcanic cloud (http://so2.gsfc.nasa.gov/Documentation/OMSO2Readme_V111_0818.htm).

3.2 OMI data analysis

The operational OMI SO_2 data products (OMSO2) are free to download from the NASA GES DISC website (http://mirador.gsfc.nasa.gov/cgi-bin/mirador/collectionlist.pl?keyword=omso2). We used the OMIplot software (Carn 2011b) to analyze them, which is written in Interactive Data Language (IDL). Several different algorithms have been used for retrieval of SO_2 from OMI measurements: the Band Residual Difference (BRD) algorithm (Krotkov et al. 2006), the Linear Fit (LF) algorithm (Yang et al. 2007), the Iterative Spectral Fitting (ITF) (Yang et al. 2009), and the Extended Iterative Spectral Fitting (EITF) (Yang et al. 2010). The LF algorithm is used for operational SO_2 retrievals, provided in the public available OMSO2 dataset.

We used the LF algorithm data in this study, which permits generation of daily maps of SO_2 vertical column densities (VCD) (http://so2.gsfc.nasa.gov) by converting the satellite slant column densities (SCD) using an air mass factor (AMF). The LF algorithm uses 10 OMI wavelengths that correlate with local maximum and minimum absorption of SO_2 (Yang et al. 2007). By making assumptions about the vertical distribution of SO_2, it provides three estimates of the SO_2 VCD in Dobson Units (1 DU = 2.69×10^{16} molecules/cm^2): the Lower Tropospheric SO_2 column (TRL), which corresponds to a center of mass altitude (CMA) of 2.5 km; the Middle Tropospheric SO_2 column (TRM), which corresponds to a CMA of 7.5 km; and the Upper Tropospheric and Lower Stratospheric SO_2 column (STL), which corresponds to a CMA of 17 km. The LF algorithm generates SO_2 VCD for these three a-priori SO_2 vertical distributions, which are then analyzed manually with the OMIplot software. The BRD algorithm is also used operationally to generate SO_2 VCDs assuming a CMA of 0.9 km, for SO_2 confined to the Planetary Boundary Layer (PBL).

Plume height was either provided by the Istituto Nazionale di Geofisica e Vulcanologia (INGV) of Catania, which monitors Mount Etna, or estimated with the READY system and the HYSPLIT trajectory model (

http://ready.arl.noaa.gov/HYSPLIT.php). Figure 3.1 is an example of the HYSPLIT trajectory model for the August 29th, 2011 paroxysm. Because the plume was covered by the row anomaly on that day, we used the OMI picture of the day after to calculate the SO_2 mass. The plume location is known with the OMI picture, at the overpass time. We then find the right plume height, the one which has a trajectory that passes above Mount Etna. The model also permits to compare the onset time of eruption. Moreover, we can see in this case that the plume height varies a lot as it is drifted away from the vent.

Once we had the plume height, we interpolated the OMI-derived SO_2 VCDs for the four CMAs to the actual reported or estimated plume altitude.

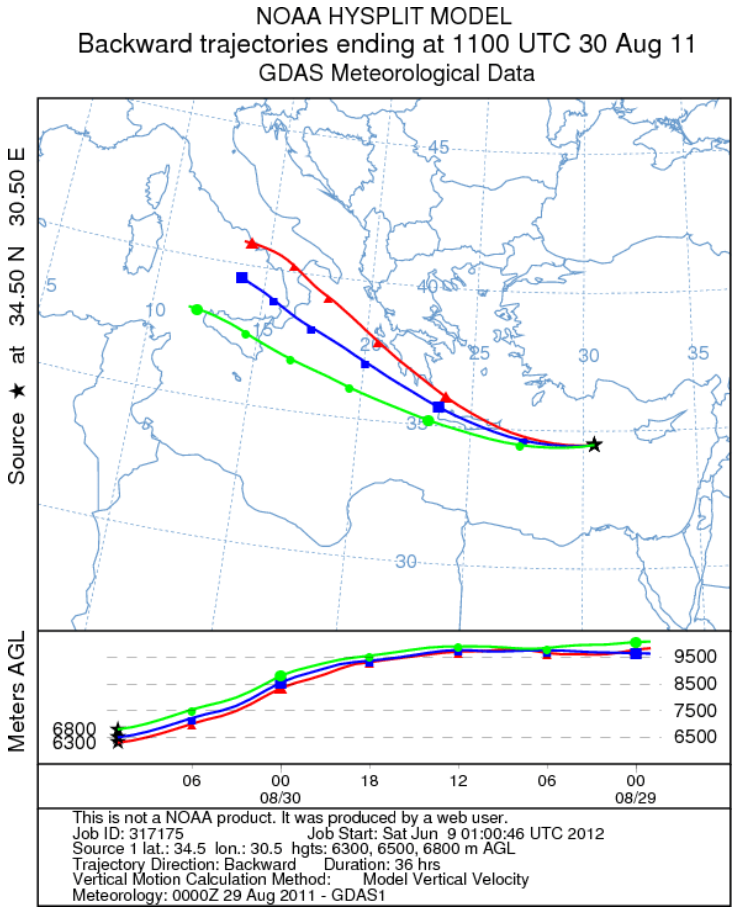

Figure 3.1: Figure from the HYSPLIT trajectory model on August 30th, 2011.

We used the Transects technique to calculate SO_2 fluxes and the Normalized Cloud-mass technique (NCM) for SO_2 mass calculation from OMI SO_2 data. These techniques are described below.

3.2.1. SO_2 Transect technique

The SO_2 transect technique is used for calculation of SO_2 fluxes in the plume from the daily OMI images. The technique is essentially the same as the technique commonly used to derive SO_2 emission rates from ground-based measurements of SO_2 column amounts in volcanic plumes (e.g. Stoiber et al. 1983). For satellite data validation during the Etna paroxysmal eruptions it is only useful for specific conditions: the eruption has to have happened a short time before the OMI image acquisition in order to have plume transects geometry and meteorological conditions similar to those of the ground-based measurements.

Transects are drawn perpendicular to the observed plume direction and the software calculates automatically the plume width and average SO_2 column in the plume cross-section. The flux is then calculated based on a wind speed entered by the user. Fluxes are obtained in metric tons per day (t/d) for the different SO_2 CMAs (PBL, TRL, TRM and STL).

3.2.2. Normalized Cloud-mass (NCM) technique

This technique consists of selecting a box in the daily OMI SO_2 image that contains the volcanic plume, in order to calculate the uncorrected SO_2 mass. Because of the OMI SO_2 background noise, another box is also selected, with a similar size and

meteorological conditions to the plume box (if possible), but free of volcanic SO_2. The NCM technique calculates the SO_2 mass of the two boxes and then subtracts the background SO_2 mass to have the corrected SO_2 mass of the volcanic plume, using the following equation:

$$SO_{2\ Cloud\ Mass} = SO_{2\ Cloud} - ((Area_{\ BG} / Area_{\ Cloud}) \times SO_{2\ BG\ Mass})$$

Where $SO_{2\ Cloud\ Mass}$ is the SO_2 mass in the volcanic plume after correction; $SO_{2\ Cloud}$ is the uncorrected SO_2 mass in the plume; $Area_{\ Cloud}$ is the area of the box containing the volcanic plume; $Area_{\ BG}$ is the area of the background box and $SO_{2\ BG\ Mass}$ the SO_2 mass (retrieval noise) in the background box. Masses are obtained in tons (t).

The NCM technique was used to estimate the SO_2 mass emitted reported in Table 2.1. For some recent eruptions, the row anomaly previously mentioned affects the OMI data coverage of the Etna plume, preventing the SO_2 mass calculation. However, if the SO_2 plume persists in the atmosphere for a few days, we were able to measure the SO_2 mass on a subsequent day.

3.2.3 Error calculation

There are different error sources for the SO_2 flux and mass calculation.

The main error sources for the flux calculation are the wind speed and the plume height. The distance measurement between the vent and the transect in the Transect technique is another error source, but minor compare to the other ones. The presence of clouds and ash are also minor errors. We estimated an error of ± 30% for SO_2 flux.

The main error source for the mass calculation is the plume height. The presence of clouds and ash are also minor errors. We estimated an error of ± 20% for the SO_2 mass.

4. Ground-based measurements

4.1 FLAME Network

The FLAME network is an automatic scanning array designed, built and installed at Etna in October 2004 by the INGV. It was composed of 5 UV scanning spectrometers (mini-DOAS) until 2009. Since 2010, 4 more stations have been added to the network to increase the probability of detecting and tracking the plume, and improve monitoring of Etna's SO_2 emissions (Figure 4.1). Data from the spectrometers are used to measure the SO_2 flux automatically and in real time (Burton et al. 2004).

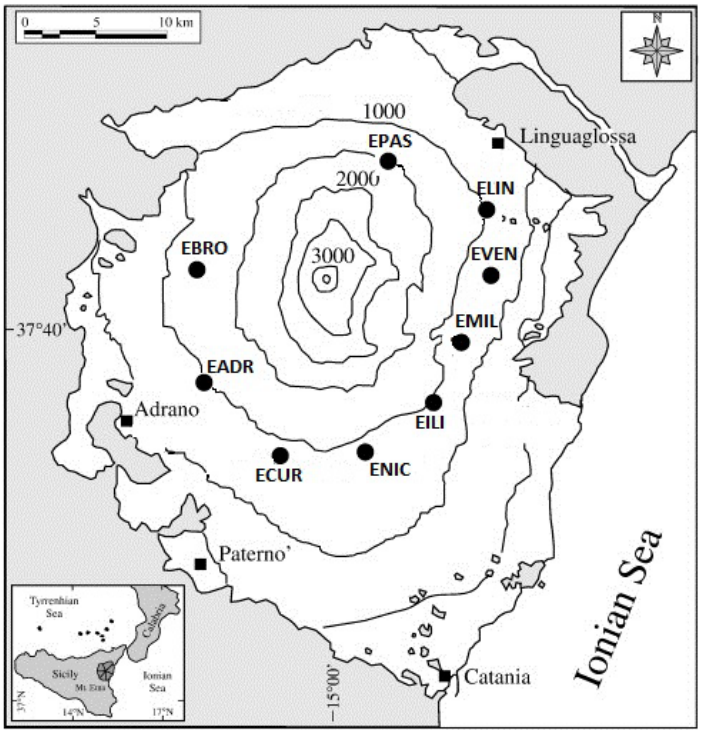

Figure 4.1: Location of the 9 UV spectrometer stations of the FLAME network. Courtesy of Istituto Nazionale di Geofisica e Vulcanologia, Osservatorio Etneo, Italy.

A filter for visible light (HOYA U330) receives the diffuse sky radiation. It is then reflected into a telescope with a 8 mrad instrumental field-of-view (FOV) by a 45º plane mirror. Fiber optic cables (1000 μm) focus the beams and connect the telescope to an Ocean Optics S2000 spectrometer. This spectrometer has a spectral resolution of 0.6-0.9 nm (full width at half maximum) and a wavelength range of 295-375 nm. The instrument scans the sky from 12º to 168º in a vertical plane in around 6 minutes, generating 105 spectra per scan (104 spectra with angular spacing of 1.5º and a dark-spectrum) (McGonigle et al. 2003; Salerno et al. 2009a, 2009b). The data acquisition period depends on the season, with almost 9 hours typical during the summer.

4.2 Mini-DOAS Data Analysis

Column amounts (CA) are retrieved automatically on site using a DOAS-type retrieval based on the Rodgers (1976, 2000) optimal estimation algorithm. Spectra are first processed with a low-pass filter in order to suppress the noise, and then transformed into optical depth. CA are calculated from the optical depth and transmitted to the INGV Observatory in Catania by FreeWave radio modem (Salerno et al. 2009a, 2009b).

Fluxes are calculated in Catania following the technique described by Stoiber et al. (1983). CAs permit calculation of SO_2 column cross-sections, which are then multiplied by the plume-transport speed. The wind speed at plume height is estimated using the LAMI model (Limited Area Model Italy) from the European Center for Medium-Range Weather Forecasts (ECMWF, http://www.ecmwf.int/) (Salerno et al. 2009b).

The INGV Observatory of Catania provided the ground-based data.

4.3 Error calculation

The uncertainty for the SO_2 flux calculation was estimated by Salerno et al. (2009b) as -22%, +30%. The Matlab code we used for the SO_2 mass calculation didn't change this error as we just integrated the fluxes to calculate the mass.

5. Results and comparison

5.1. OMI Results

5.1.1. Transects Technique

The cloud fraction image provided by OMIplot permits an assessment of the presence or absence of significant meteorological cloud at the volcanic plume location (Figure 5.1). Depending on the relative position of clouds and the volcanic plume, the SO_2 mass calculated may be overestimated (if the SO_2 is above the clouds) or underestimated(if the cloud is obscuring part or all the SO_2 plume). Furthermore, they can modify the rate of SO_2 depletion via aqueous phase reactions, leading to an underestimation of SO_2 if the volcanic plume is entrained into cloud (Jaeschke et al. 1982). Therefore, cloud coverage is an important parameter to take into account.

The OMI-derived cloud fraction is available for any single pixel and the OMSO2 data product also provides a cloud top pressure. It is then possible to calculate the estimated height of the cloud and compare it with the (known or estimated) volcanic plume height. We used the U.S. Standard Atmosphere, 1976 published by the U.S. Government Printing Office, Washington, D.C. (http://www.pdas.com/m1.html) to estimate the cloud height.

Visible images from the Moderate Resolution Imaging Spectroradiometer (MODIS) on the Aqua satellite are also useful to assess cloud coverage as the sensor is in the A-train satellite constellation with Aura and overpasses the area a few minutes before OMI (http://lance-modis.eosdis.nasa.gov/imagery/subsets/?project=aeronet&subset%20=ETNA) (Figure 5.2).

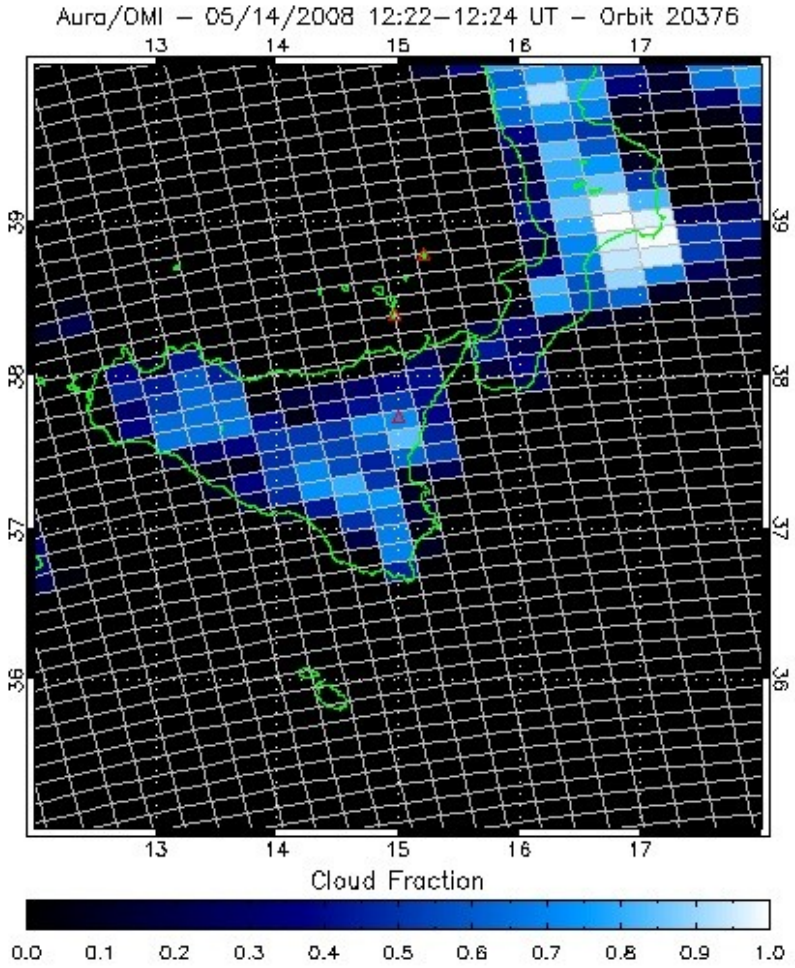

Figure 5.1: Cloud fraction image on 05/14/08.

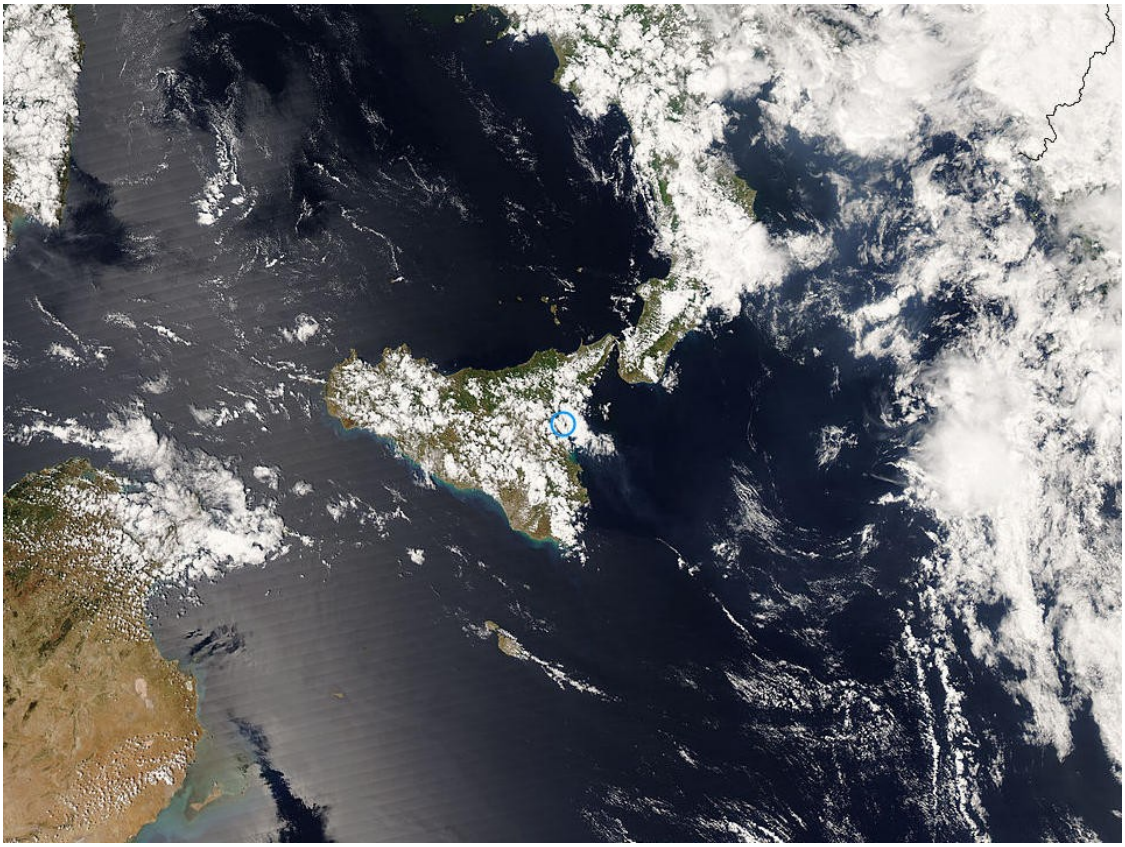

Figure 5.2: Aqua MODIS image above Sicily on 05/14/08. The blue circle is the Etna location.

Figures 5.1 and 5.2 show a good agreement in cloud locations. The volcanic plume is also visible on the Aqua image, drifted South-East by the wind.

The INGV provided the wind speed at the location of the ground-based stations. As it can easily vary as the plume drifts away, we used the READY Hysplit model to have another value of it. The Archived Meteorology data provides an estimation of the wind speed depending on the location and altitude (http://ready.arl.noaa.gov/READYamet.php). The READY Trajectory model was also used to compare the results. It gives us the onset and end times of the eruption. These combined with the plume length calculated with OMIplot, allow us to have another

estimation of the wind speed. The most true value was used to calculate the flux, depending on the location of the transect.

The plume height can be found for some eruptions in the INGV reports of activity (http://www.ct.ingv.it/index.php?option=com_docman&Itemid=344&lang=it). However, this is the height at the vent, and as the plume drifts away, the altitude might change. We used the READY Trajectory model to have another estimation of the height at the plume location.

Wind speed and plume height are two important parameters as they are used in the flux calculation. When these two data sets are more accurate, the approximation for flux is more accurate.

The OMIplot distance calculation technique was used to calculate the distance between each transects and the vent. Using the wind speed data, we were then able to calculate the corresponding time range of the flux emission.

Figures 5.3 to 5.6 show the transect images of the days used for the comparison.

We didn't calculate flux too close from the volcano. Indeed, because of the large OMI pixel size, the plume needs to have dispersed enough to cover a sufficient fraction of it, and avoid an underestimation of SO_2.

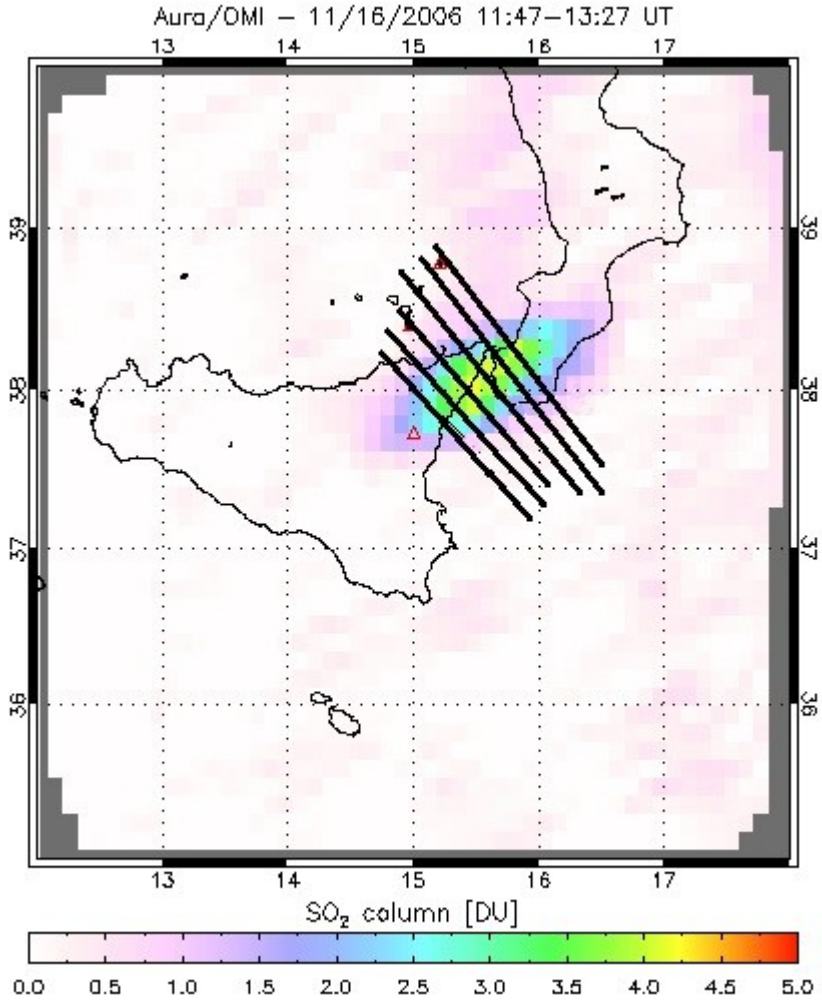

Figure 5.3: OMI picture with transects used to calculate the SO_2 fluxes for the 11/16/06 paroxysmal event.

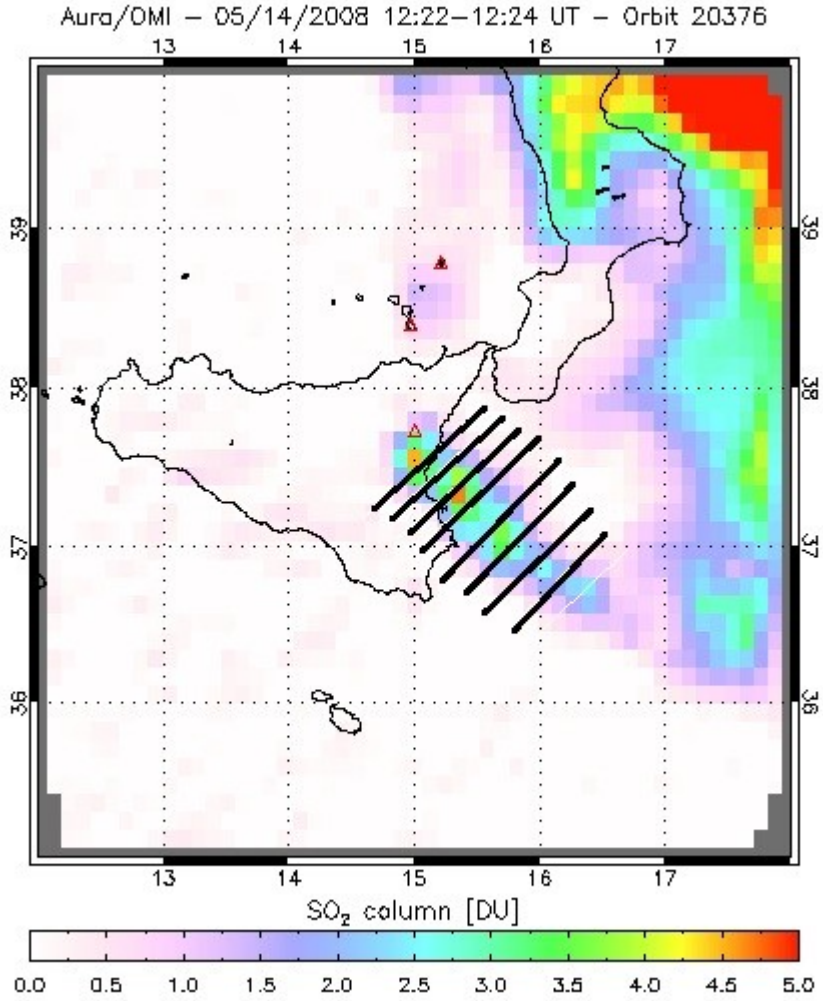

Figure 5.4: OMI picture with transects used to calculate the SO_2 fluxes for the 05/14/08 paroxysmal event.

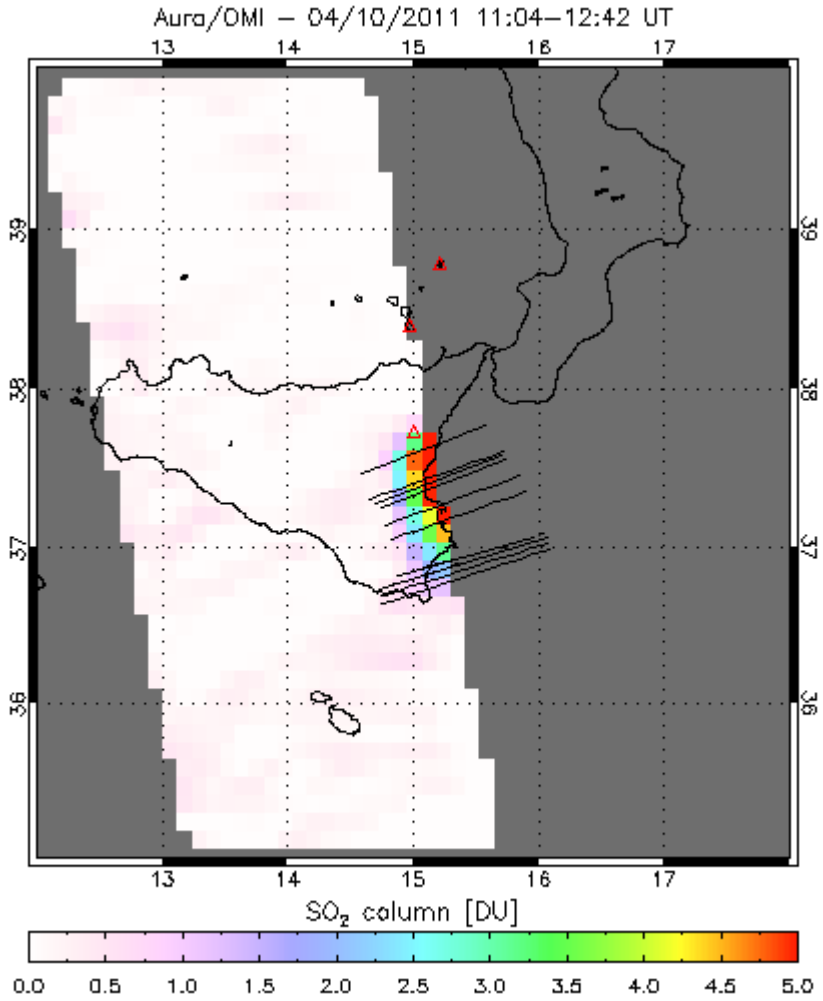

Figure 5.5: OMI picture with transects used to calculate the SO_2 fluxes for the 04/10/11 paroxysmal event.

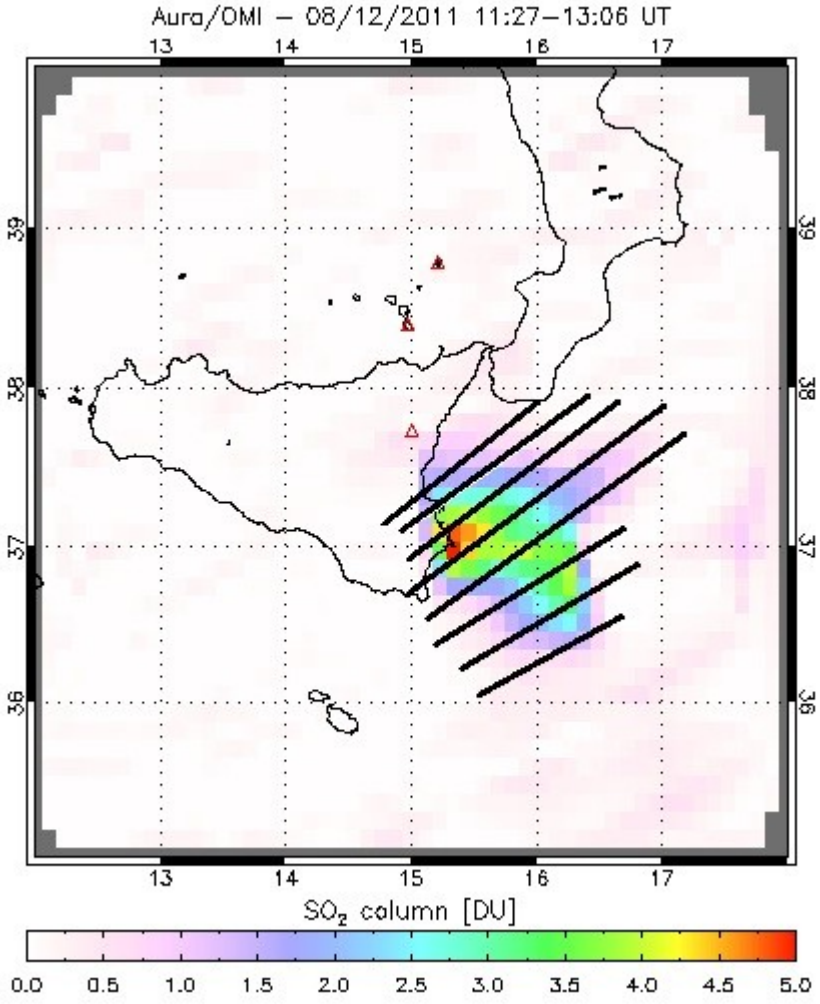

Figure 5.6: OMI picture with transects used to calculate the SO_2 fluxes for the 08/12/11 paroxysmal event.

5.1.2. Cloud-Normalized Mass Technique

The CNM technique was used to calculate the SO_2 mass. As described before, we chose two different boxes, one with the volcanic plume and one for the background (figures 5.7 to 5.10).

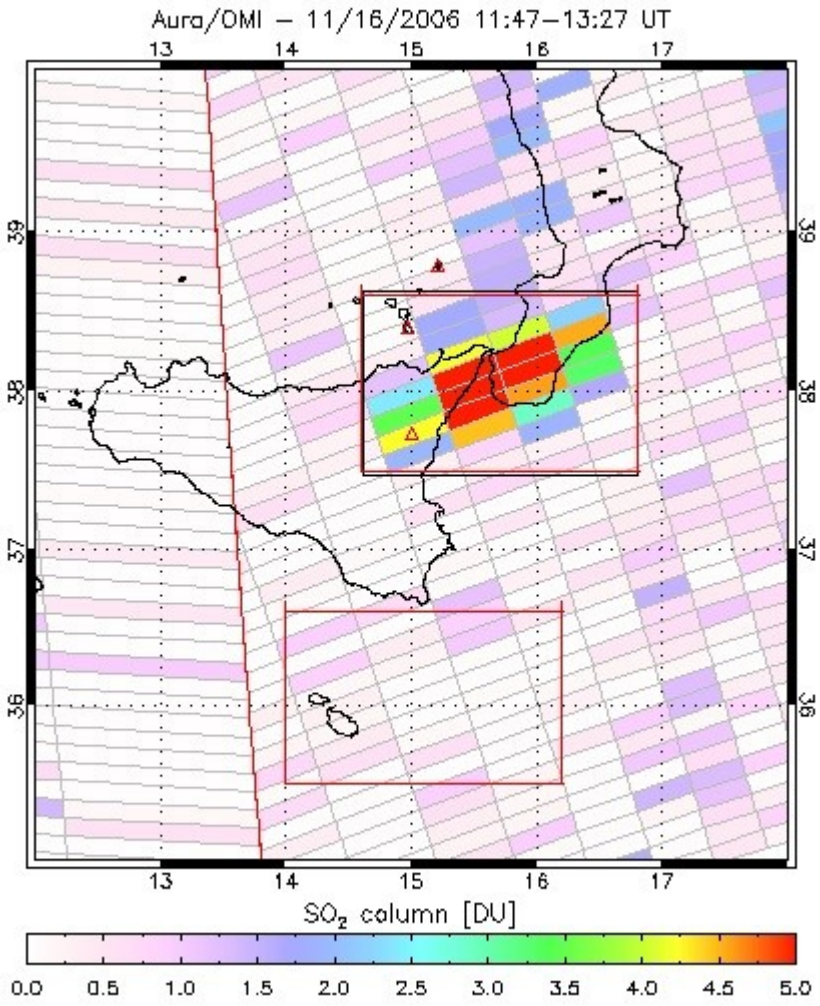

Figure 5.7: OMI image with the boxes used for the SO_2 mass calculation on 11/16/06 paroxysmal event.

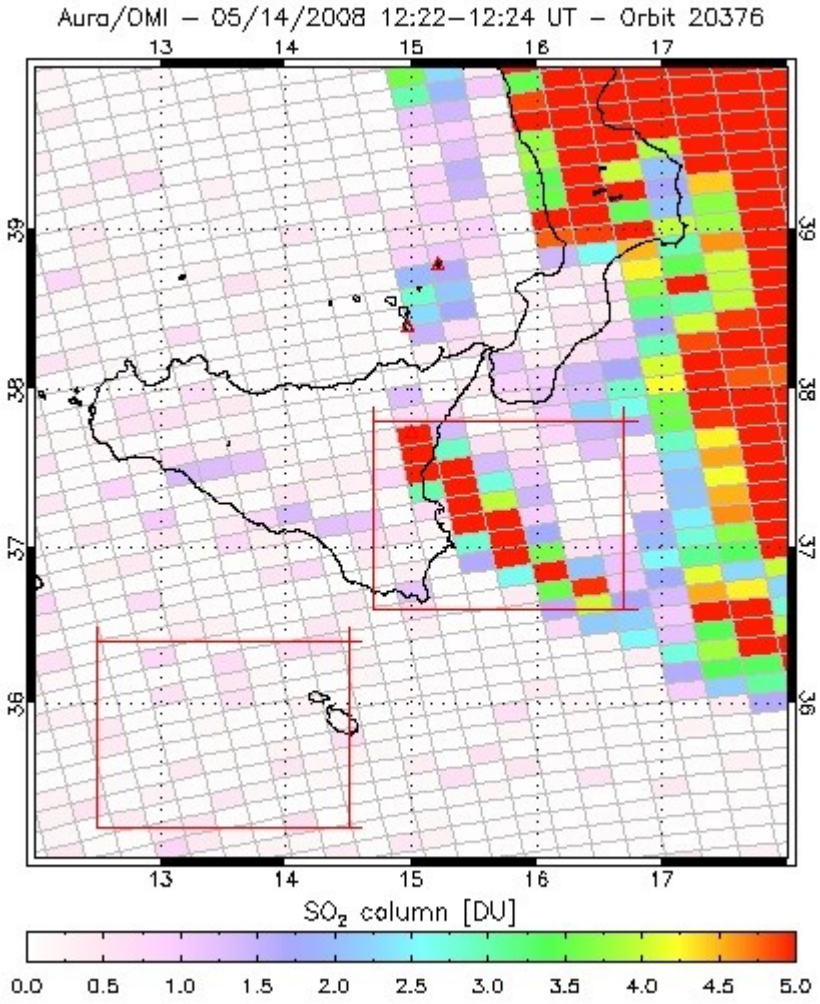

Figure 5.8: OMI image with the boxes used for the SO_2 mass calculation on 05/14/08 paroxysmal event.

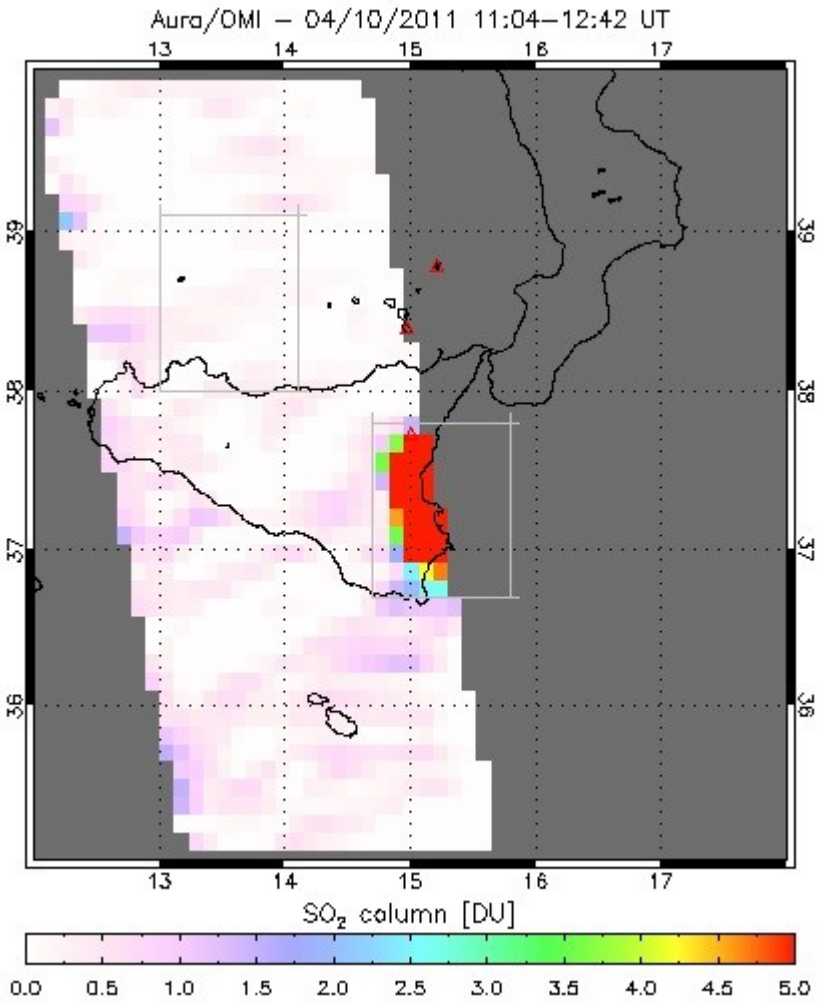

Figure 5.9: OMI image with the boxes used for the SO_2 mass calculation on 04/10/11 paroxysmal event.

The grey bands in Figure 13 are the row anomaly. We can see that it cuts a part of the volcanic plume, which means there is no data for this part. It is, in this case, really important to take it into account for the SO_2 flux and mass calculation.

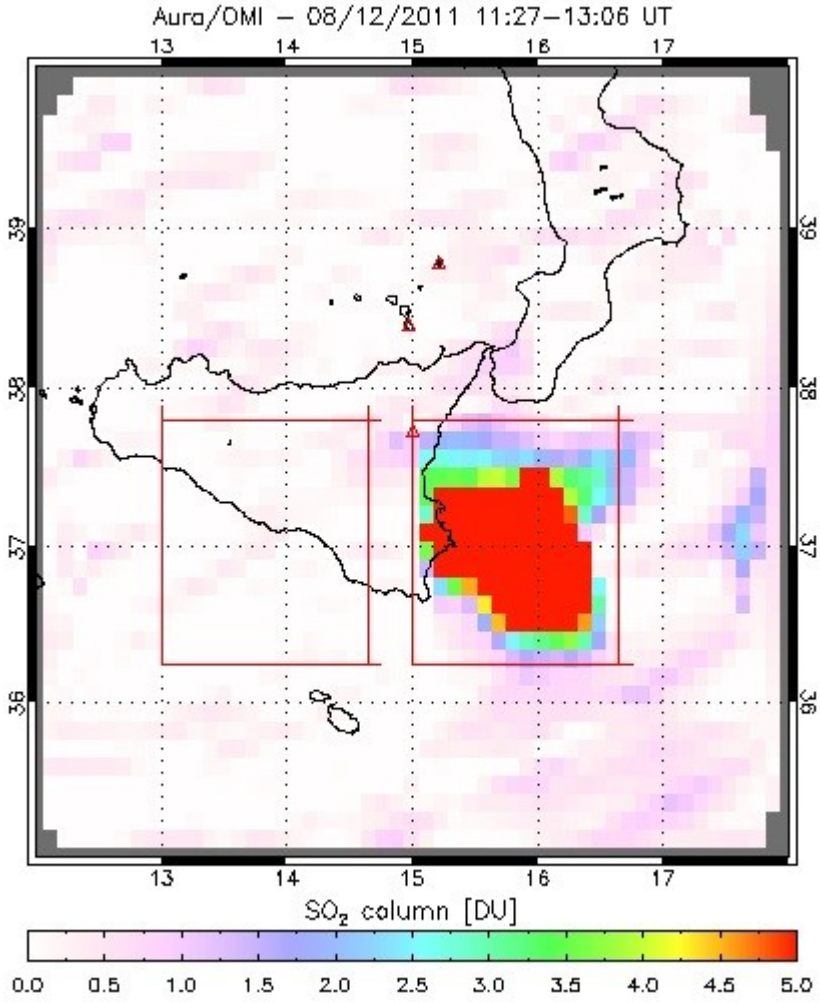

Figure 5.10: OMI image with the boxes used for the SO_2 mass calculation on 08/12/11 paroxysmal event.

The July 9th, 2011 eruption occurred in the afternoon, after the OMI overpass above Mount Etna. We calculated the SO_2 mass of the volcanic plume using the image of July 10th, so that almost 24 hours after the emission (Figure 5.11). We see on the picture that the end of the plume is cut by the row anomaly. However, we were able to estimate with HYSPLIT that a very short part of the plume is cut by the anomaly. The SO_2 mass calculated is then very close to the real one. This technique allows us to compare data for events which occur during the afternoon. However, because of the lapse time, an underestimation of SO_2 is most likely due to its oxidation into sulfate aerosols.

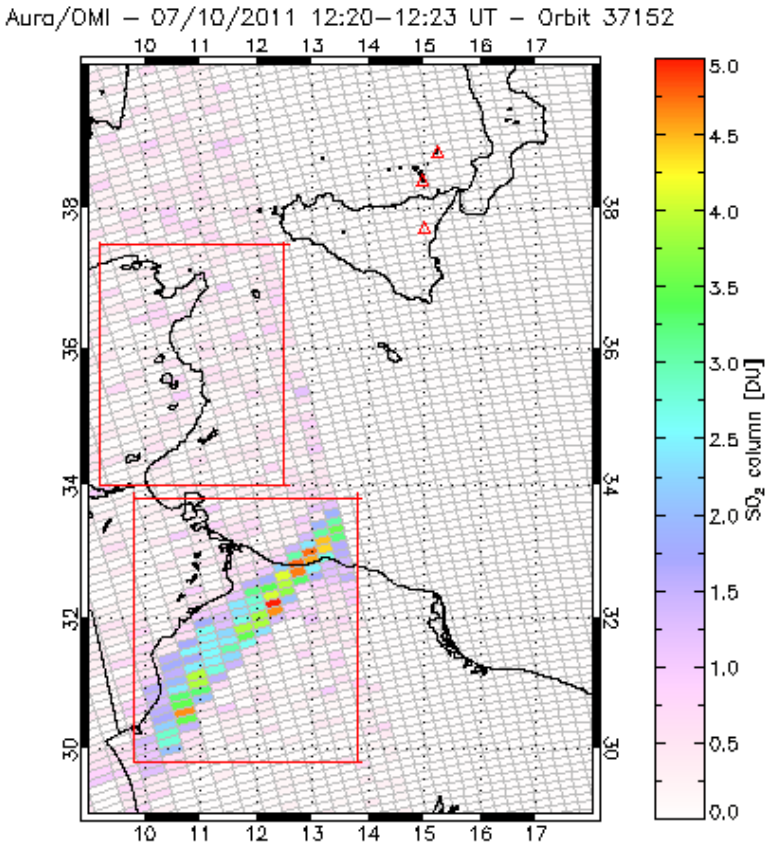

Figure 5.11: OMI image with the boxes used for the SO_2 mass calculation on 07/09/11 paroxysmal event.

5.2. Ground-based results

The SO_2 fluxes were provided by the INGV of Catania with the wind speed at the station location. For each flux calculated with OMIplot, we had the corresponding time of emission. Because the distance between the transects and the vent and the wind speed values are not hundred percent accurate, we calculated an average of the DOAS fluxes for the comparison, ± 10 minutes of the flux emission time. We also reported the maximum and minimum fluxes during this time lapse in our comparison.

We estimated the SO_2 mass erupted for each paroxysmal event with a Matlab code. SO_2 fluxes from the beginning of the eruption until its end were integrated in order to have the SO_2 mass erupted during this time lapse.

5.3. Comparison

The conditions were adequate for comparisons of both flux and mass between the OMI and FLAME measurements for four paroxysmal events during the period 2004 to present. Because of its occurrence in the afternoon, only the mass comparison was possible for a fifth eruption.

5.3.1. November 16th, 2006

The November 16th, 2006 eruption occurred between 04:07 and 14:00 GMT. As the FLAME network only measures during daytime, there is no ground-based data for the beginning of the event. The first measure was at 07:39, so we compared the data from this time to the OMI overpass time, at 13:27. The data for this day are presented in Table 5.1 and plotted in Figure 5.12.

Considering the plume height at 4 km, we used the TRL and TRM values to calculate the SO_2 fluxes and total SO_2 masses.

The conditions for this day were quite favorable, with an almost constant wind-speed, between 4.67 m/s and 6.18 m/s, and a cloud-free background. However, the satellite was not near nadir, so had larger pixel dimensions.

Table 5.1

SO_2 fluxes in t/d obtained by OMI transects and Mini-DOAS on 11/16/06.

Transect	Distance from the vent (km)	OMI	DOAS Average	DOAS Maximum	DOAS Minimum	% Difference
1	17	3064.44	5419.38	5824.05	5208.65	43.45
2	29	3922.84	6951.55	7615.45	6381.28	43.57
3	44	4915.37	8079.29	8254.72	7820.51	39.16
4	60	5421.08	11080.97	11157.76	11002.05	51.08
5	75	5427.74	10032.57	10231.55	9843.55	45.90
6	92	5528.00	8270.64	9293.61	7472.14	33.16

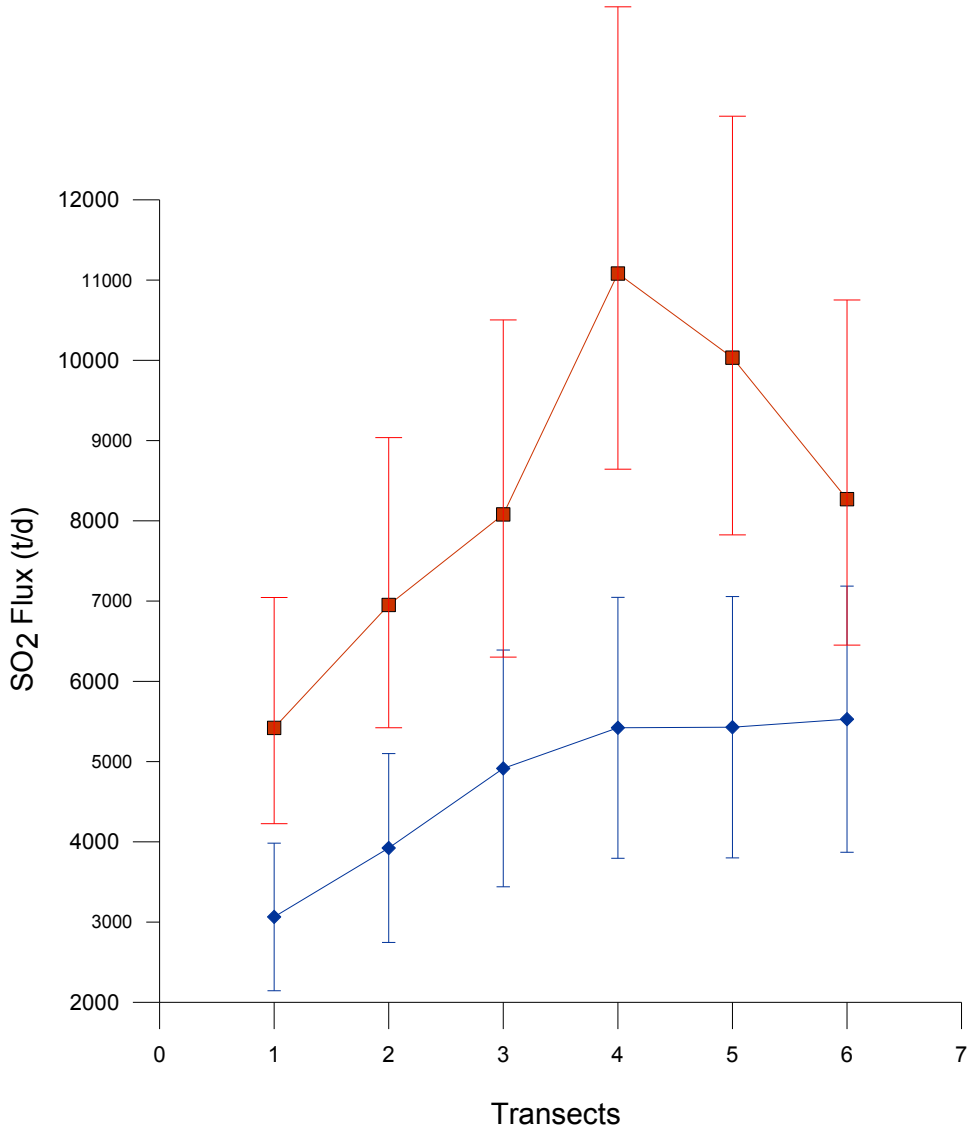

Figure 5.12: SO_2 fluxes obtained by OMI transects, blue line, compared to SO_2 fluxes obtained by Mini-DOAS, red line, on 11/16/06. The DOAS value is the average flux of the 20 minutes around the OMI flux emission time.

The two curves in Figure 5.12 show a same trend, an increase of SO_2 fluxes with the distance from the vent. However, the results show a disagreement, with the best OMI estimation 33% smaller for transect 6. Various errors could account for this difference.

The first cause must be an error ranging between 5% and 20% for the Mini-DOAS measurements (Edmonds et al, 2003), depending on the SO_2 concentration of the plume and the background noise, and varying during the day. Furthermore, clouds may have been present earlier in the morning, leading to erroneous values of Mini-DOAS fluxes. However, the underestimation is around 40% for all the results, which rules out those errors, more or less important depending on the time. The wind speed and/or the plume height estimations are then the most likely errors.

Table 5.2 presents the total SO_2 masses calculated with both techniques. In opposition to the fluxes, the OMI value is 64% larger than the DOAS one. This could be explained by the fact that the eruption starts at 04:07 GMT and DOAS measurements at 07:39. The OMI picture takes into account the SO_2 erupted from the beginning of the eruption whereas the Mini-DOAS starts measuring more than three hours later. We estimated the fluxes from 04:07 until 07:39 for Mini-DOAS and obtained a SO_2 mass closer than the OMI mass.

Table 5.2

Total SO_2 mass in tons obtained by OMI CNM technique and Mini-DOAS on 11/16/06. The second row is with the SO_2 flux estimation for DOAS.

OMI	DOAS	% Difference
1452.40 ± 290.48	887.23 -195.19, +266.17	63.70
1452.40 ± 290.48	1090.90 -240.00, +327.27	33.14

5.3.2. May 14th, 2008

We compared the SO_2 fluxes from the beginning of the DOAS measurements, at 05:47 GMT until the OMI overpass at 12:24. As said before, some clouds were present above Sicily around noon. However, the cloud fraction is very low, 0.84% for transect 1 and 0.25% for transect 2. The cloud altitude estimated with the U.S. Standard Atmosphere, 1976, is 4-5 km and 5-6 km respectively. The plume height at the vent is 4 km, which means that the volcanic plume is either mixed or under the clouds, which could lead to an underestimation of SO_2. As there is no cloud above the Ionian Sea, the other transects are not affected by this possible error.

The wind speed given by the INGV was almost constant at the vent, ranging between 6 m/s and 7 m/s and the satellite near nadir. The wind speed obtained with the READY Trajectory model was however a bit lower, around 5.5 m/s.

The plume height varies, around 4 km at the vent and 5 km at its end.

Table 5.3

SO_2 fluxes in t/d obtained by OMI transects and Mini-DOAS on 05/14/08.

Transect	Distance from the vent (km)	OMI	DOAS Average	DOAS Maximum	DOAS Minimum	% Difference
1	21	14135.33	7430.87	7698.69	7161.89	90.22
2	29	9791.38	10819.58	11888.16	10140.34	9.50
3	47	5977.24	11278.95	11831.39	10726.50	47.01
4	58	4478.01	12119.31	13174.50	11064.12	63.05
5	86	3028.77	15030.79	15910.99	14150.59	79.85
6	106	3095.05	11723.60	12853.04	10502.62	73.60
7	119	2187.77	5139.90	5553.04	4724.16	57.44
8	145	2013.07	4075.89	4826.28	2813.78	50.61

The error difference is very high for all the transects except the second and OMI fluxes are always smaller than DOAS fluxes except for the first transect (Table 5.3). As showed in Figure 5.13, OMI fluxes decrease when DOAS fluxes tend to increase. This gap could be explained by an erroneous wind speed. The strongest fluxes occurred later for OMI than for DOAS. As there is no information about the onset time of the eruption, we were just able to estimate it with the READY Trajectory model, around 05:00 GMT.

The total SO_2 mass is almost the same for both techniques (Table 5.4). The DOAS measurement began at 05:47, less than an hour after the estimated onset of the eruption. Furthermore, fluxes are generally weak at the beginning of an eruption and tend to have a normal distribution. As a result, the SO_2 mass from DOAS must be a little bit higher, then closer than the OMI one.

The good agreement between SO_2 masses reinforces the fact that the gap between the strongest fluxes may be due to an erroneous wind speed. If the masses are in the same range, fluxes should not be that different.

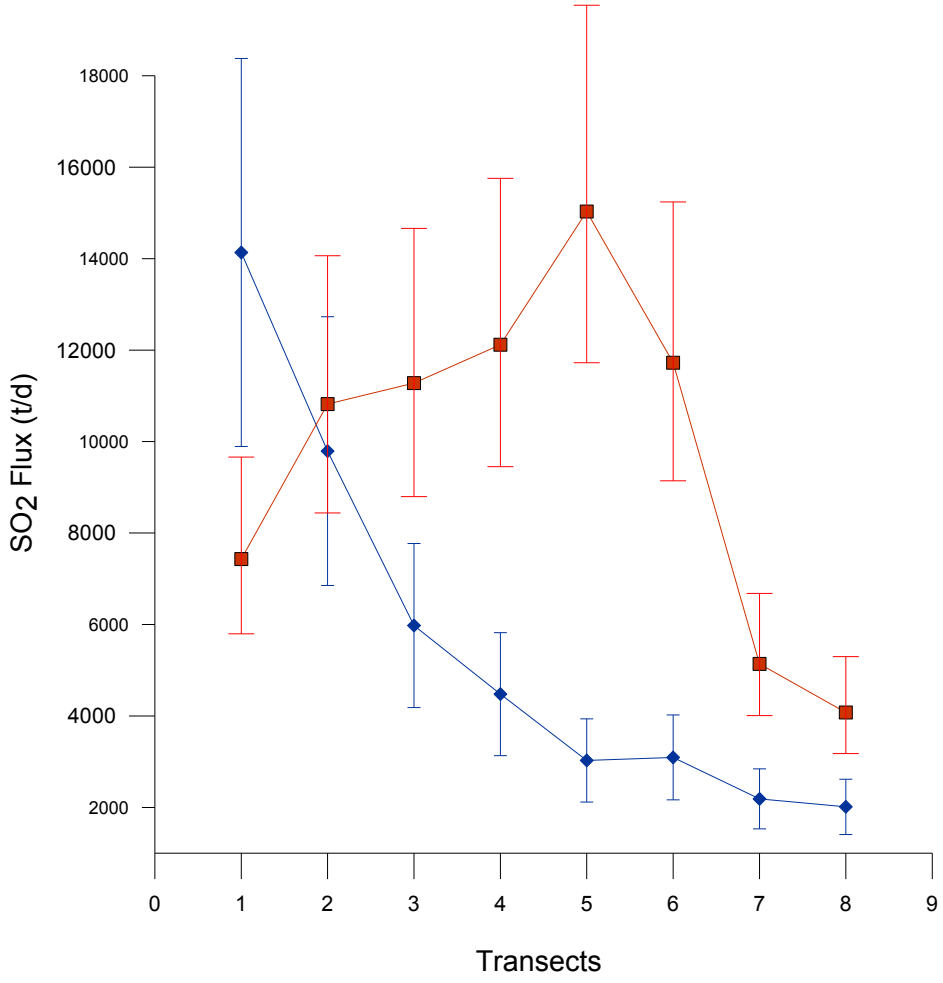

Figure 5.13: SO_2 fluxes obtained by OMI transects, blue line, compared to SO_2 fluxes obtained by Mini-DOAS, red line, on 05/14/08. The DOAS value is the average flux of the 20 minutes around the OMI flux emission time.

Table 5.4

Total SO_2 mass in tons obtained by OMI CNM technique and Mini-DOAS on 05/14/08.

OMI	DOAS	% Difference
1754.00 ± 350.80	1637.00 -360.14, +491.10	7.15

5.3.3. April 10th, 2011

We compared the SO_2 fluxes from the beginning of the DOAS measurements, at 07:19 GMT until the OMI overpass at 12:42. A part of the volcanic cloud is cut by the ROW anomaly for that day. Comparing the image with the anomaly (Figure 5.14) and the one with the estimated plume (Figure 5.15) allows us to assume that around half of the plume is covered by the anomaly. Furthermore, the shape of transects obtained by the CNM technique reinforces this hypothesis. Figure 5.16 shows the transect 6. We found with the distance calculation tool from OMIplot, that the plume width is around 80 km at this location. We see in the figure that the plume is cut at the highest SO_2 amount, and around 43 km from the west edge, which is almost half of its width.

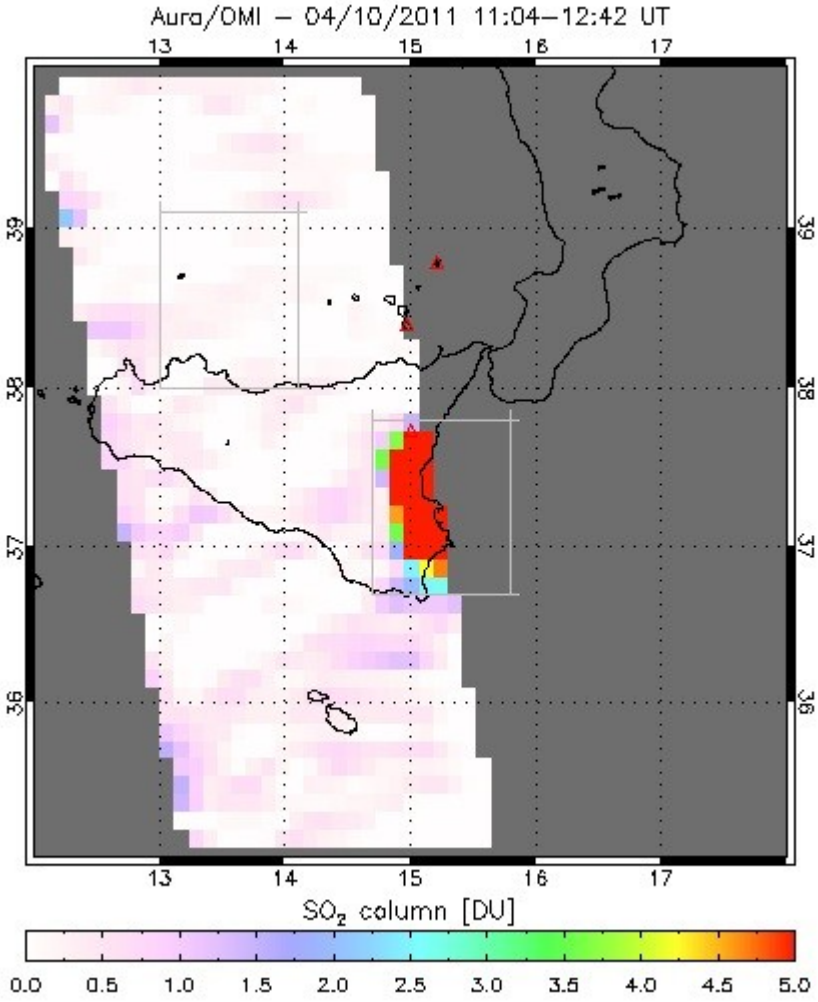

Figure 5.14: OMI picture with the ROW anomaly on 04/10/11.

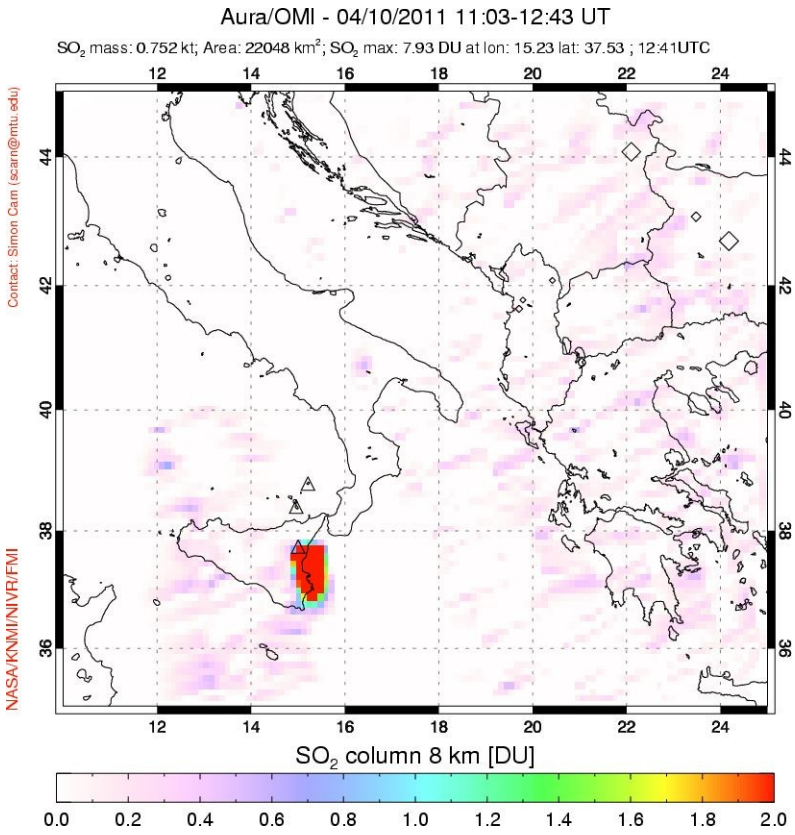

Figure 5.15: OMI picture without the ROW anomaly on 04/10/11.

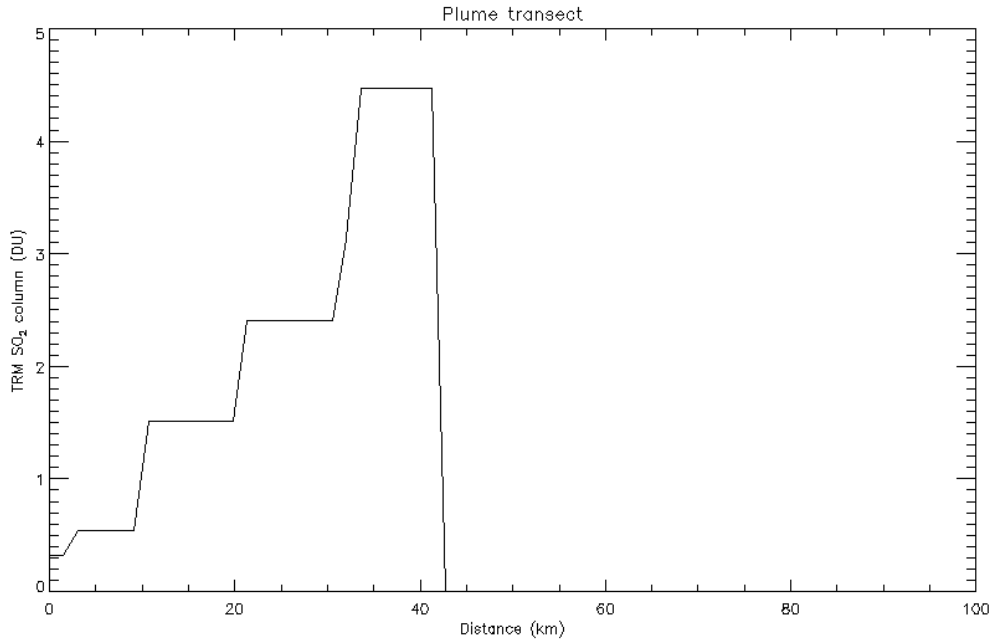

Figure 5.16: Plume transect for transect 6 on 04/10/11.

The conditions were favorable, with a cloud-free background. The wind speed at the vent varies from 6.7 to 8.3 m/s. However, the wind speed estimated with READY is a little bit higher, around 9 m/s, which is also closer to the one calculated with the plume length and duration of the emission. We used this value of 9 m/s for the OMI flux calculation. The plume height given by the INGV is 5.3 km, which is consistent with the one estimated by the trajectory model.

Table 5.5

SO_2 fluxes in t/d obtained by OMI transects and Mini-DOAS on 04/10/11.

Transect	Distance from the vent (km)	OMI	OMI*2	DOAS Average	DOAS Maximum	DOAS Minimum	% Difference
1	18	4191.88	8383.76	8582.96	10084.82	6958.71	2.32
2	41	6430.93	12861.86	12479.15	14604.33	10277.14	3.07
3	45	5739.70	11479.41	14009.73	15382.56	11524.14	18.06
4	49	5167.10	10334.19	14521.67	15482.66	13667.55	28.84
5	57	3807.19	7614.37	11026.48	13156.89	9266.87	30.94
6	70	3407.86	6815.71	9104.01	9676.80	8222.14	25.14
7	107	1392.21	2784.42	1961.28	2013.64	1726.33	41.97
8	112	1195.76	2391.52	2004.15	2365.79	1726.33	19.33
9	117	964.39	1928.78	2237.18	2625.11	1979.47	13.79
10	122	669.29	1338.58	1919.11	2095.48	1834.42	30.25

Assuming that half of the plume is covered by the row anomaly, we multiplied the OMI data by two before comparing. As showed in Table 5.5, the best agreement is for transects 1 and 2, with a low percent difference, 2.32 and 3.07 respectively. Transects 3, 8 and 9 also show a decent agreement, with percent difference inferior to 20. Furthermore, the two curves on Figure 5.17 have the same trend and OMI fluxes on the range of DOAS fluxes for transects 1, 2, 3, 9 and 10.

The SO_2 masses are also really close (Table 5.6), with only 2.95 percent difference, calculated from 08:00 GMT, beginning of the event, until 12:43, overpass of the satellite.

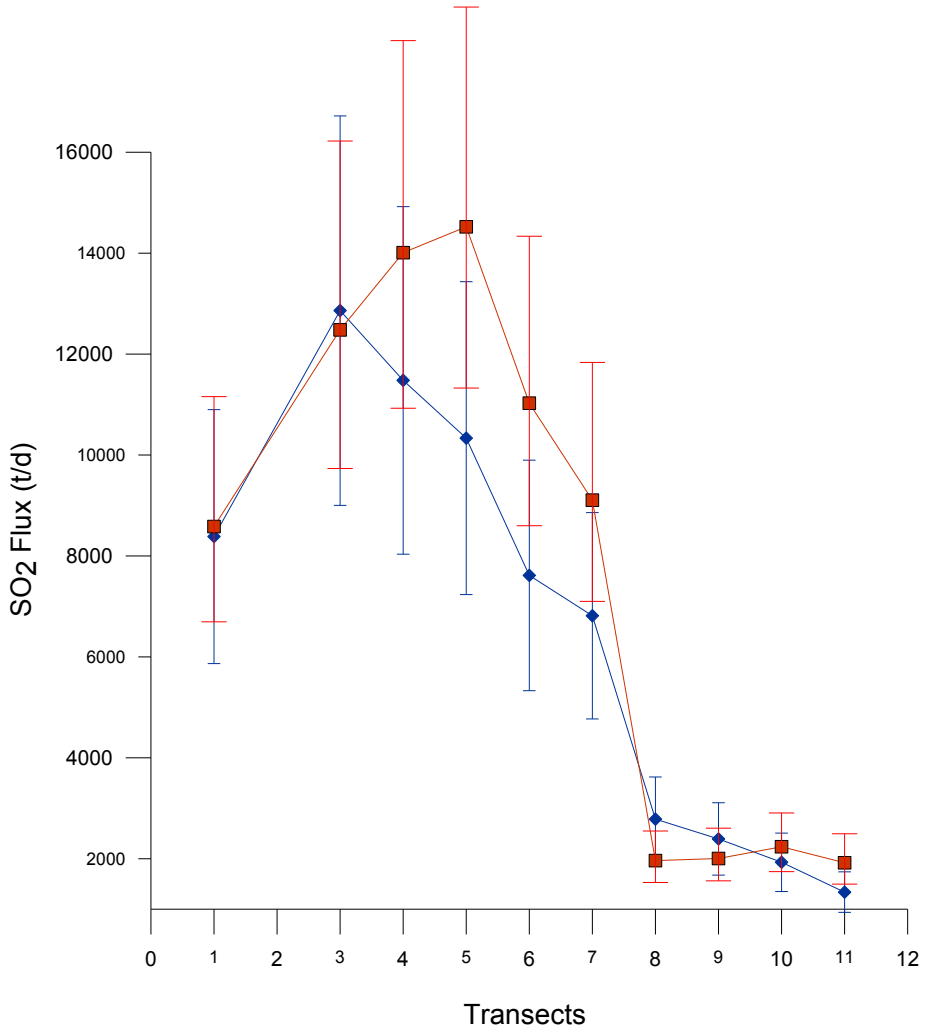

Figure 5.17: SO_2 fluxes obtained by OMI transects, blue line, compared to SO_2 fluxes obtained by Mini-DOAS, red line, on 04/10/11. The DOAS value is the average flux of the 20 minutes around the OMI flux emission time.

Table 5.6

Total SO_2 mass in tons obtained by OMI CNM technique and Mini-DOAS on 04/10/11.

OMI	OMI * 2	DOAS	% Difference
768.80	1493.60 ± 307.52	1537.60 -328.59, +448.08	2.95

5.3.4. August 12th, 2011

The paroxysmal event on August 12th, 2011 occurred between 07:00 and 11:30 GMT, during daytime and before the OMI overpass, with a cloud-free background and a plume height around 3.7 km. These conditions are favorable for the comparison. However, the satellite is not near nadir, and the average wind speed at the vent is very different from the one at the plume location, 4.9 m/s and ~8 m/s respectively. There is then a big difference between the wind speeds used to calculate DOAS and OMI fluxes.

The results presented in Table 5.7 and plotted in Figure 5.18 show a big difference between the fluxes, with OMI estimation being ~ 300% larger, and until 1058% larger for transect 6. Transect 1 is the only one under 100% larger. The trend is the same for the mass comparison, with 502 percent difference (Table 5.8).

Table 5.7

SO_2 fluxes in t/d obtained by OMI transects and Mini-DOAS on 08/12/11.

Transect	Distance from the vent (km)	OMI	DOAS Average	DOAS Maximum	DOAS Minimum	% Difference
1	36	2818.26	1536.11	2225.88	1052.76	83.47
2	55	8103.45	1920.91	3427.85	1321.31	321.85
3	69	18365.24	3591.23	5010.16	2045.37	411.39
4	94	14948.17	3483.89	3810.79	2987.05	329.07
5	114	18434.54	5388.92	6372.85	4734.96	242.08
6	136	17189.70	1484.21	2778.73	826.50	1058.17

As showed in Figure 5.18, OMI fluxes are, except for transect 1, never in the range of DOAS fluxes. This eruption is characterized by pulsating lava fountains 100m high for two hours and strong strombolian activity at the beginning and end of the event. If we compare with the DOAS data of the other eruptions, fluxes are usually between 6000 t/d and 14000 t/d during fountaining activity while they are between 2000 t/d and 5000 t/d on that day. We can assume that the DOAS data were underestimated. Indeed, accuracy of fluxes depends on the geometry of the plume and constancy of the plume transport direction. Their variation can lead to under or overestimation from -22% to +36% (Salerno et al. 2009b). The plume also might have been at the spatial limit of the scanner-network, with only part of it on the field of view.

The OMI picture (Figure 5.10) shows a plume drifted toward two main directions, east and south-east, which highlights a variation of the plume transport direction with time. The geometry of cloud could then be affected, resulting in erroneous fluxes. As said before, wind speed estimated with READY is much higher than the one given by the INGV. A wrong wind speed and/or plume height also may account for the discrepancy.

On the other hand, we measured fluxes by drawing transects in the OMI picture, with a plume that has not the same shape as near the vent when DOAS fluxes are measured. The volcanic cloud is dispersed by the variation of wind direction and an overestimation of SO_2 by OMI is likely.

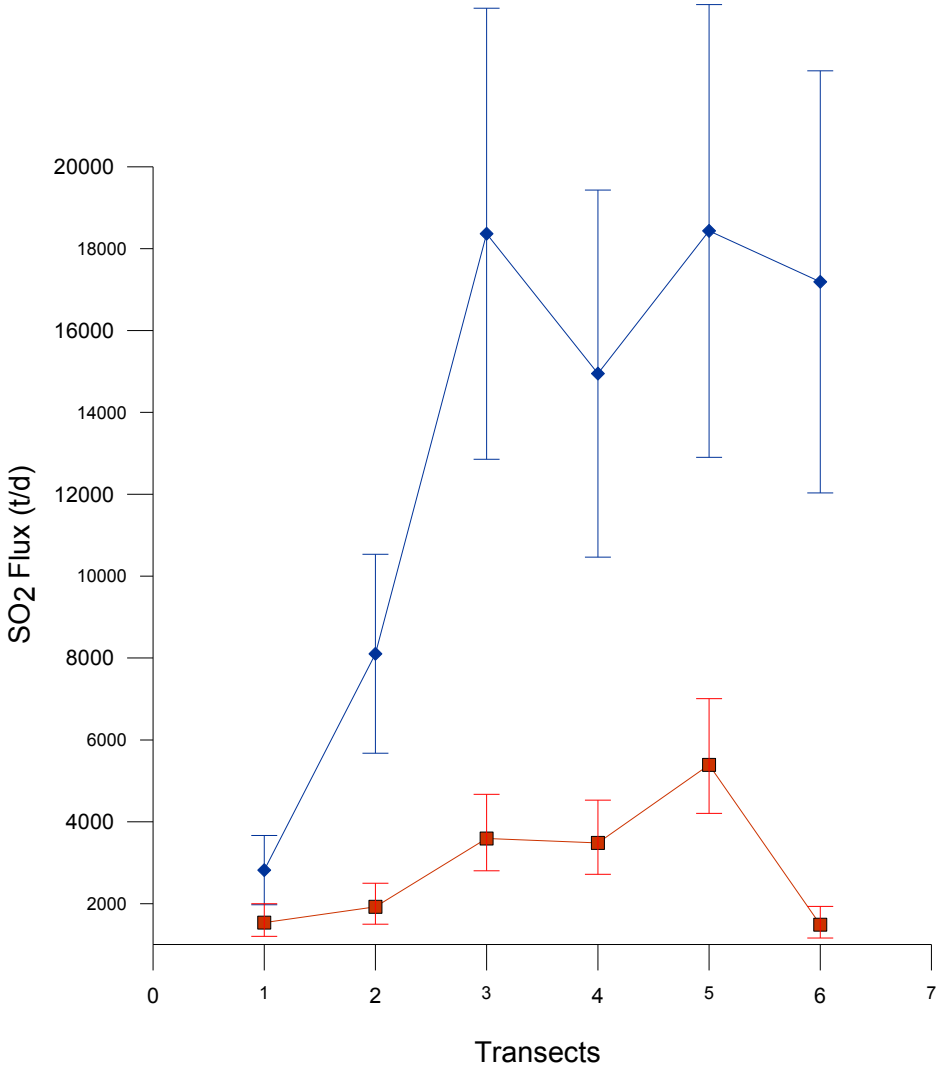

Figure 5.18: SO_2 fluxes obtained by OMI transects, blue line, compared to SO_2 fluxes obtained by Mini-DOAS, red line, on 08/12/11. The DOAS value is the average flux of the 20 minutes around the OMI flux emission time.

Table 5.8

Total SO_2 mass in tons obtained by OMI CNM technique and Mini-DOAS on 08/12/11.

OMI	DOAS	% Difference
3367.60 ± 673.52	559.86 -123.17, +167.96	501.51

5.3.5. July 9th, 2011

The July 9th, 2011 eruption occurred from 12:15 to 16:40 GMT according to the INGV report, with a plume height of 6.8 km and a cloud-free background.

As the eruption occurred after the OMI overpass on July 9th, we had to process the image of the following day. It was then not possible to make a flux comparison.

We assumed that the OMI SO_2 mass takes into account SO_2 emission from 12:15 to 16:40. DOAS measurements stop at 16:21, while fluxes are still high, ~ 5700 t/d. We calculated the DOAS SO_2 mass assuming the fluxes from 16:21 until 17:00 (Figure 5.19). The result shows a better agreement with OMI, even if the percent difference is still 35.57 (Table 5.9).

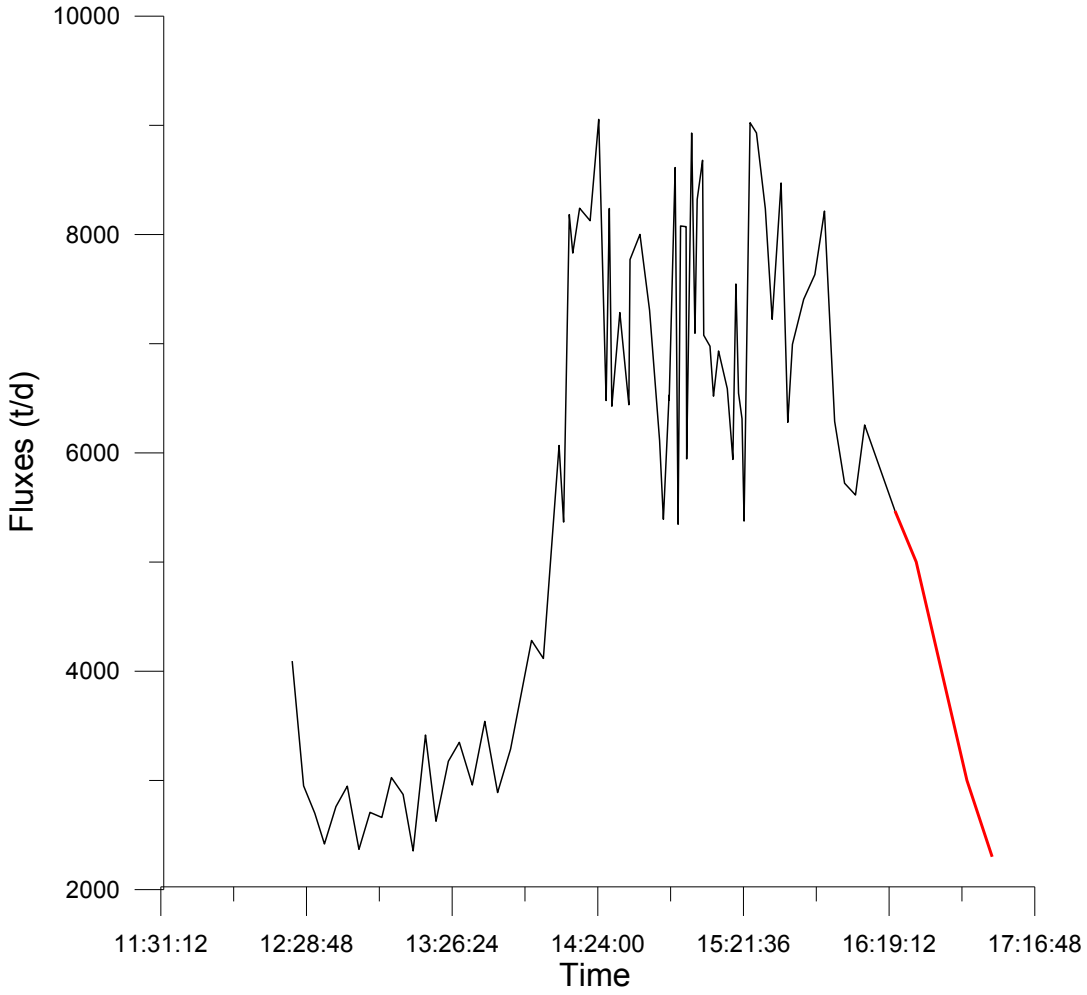

Figure 5.19: DOAS flux versus time graph on 07/09/11. The red line is the assumed trend of the curve when DOAS measurement stops.

Table 5.9

Total SO_2 mass in tons obtained by OMI CNM technique and Mini-DOAS on 07/09/11. The second line shows the SO_2 mass calculated with DOAS data until 17:00.

OMI	DOAS	% Difference
1747.56 ± 349.51	1224 - 269.28, +367.20	42.77
1747.56 ± 349.51	1289 - 283.58, +386.70	35.57

6. Conclusion

This kind of comparison between satellite and ground-based sensors is always tricky as it requires finding overlapping ground-satellite days. In the case of Mount Etna, it was really challenging as the OMI satellite has an overpass time around 12:45. Only the events that occurred in the morning were comparable, as the FLAME network, having UV-spectrometers using sun radiation, does not measure during nighttime. The afternoon eruptions could be compared if the volcanic plume was still visible the day after, with a likely SO_2 underestimation due to chemical reactions in the atmosphere.

Although Mount Etna is a very active volcano, especially since the beginning of 2011, it was difficult to find good data for both sensors. Furthermore, the degassing rate is not big enough to be detected by the OMI satellite, so only the paroxysmal events were used for the comparison. Out of eleven days of Mini-DOAS data, only five of them were comparable with the OMI data.

The row anomaly present in the northern hemisphere since June 2007 was another difficulty as it often appears to be above the volcano, preventing the use of OMI data.

Otherwise, there were only five ground-based stations until 2010, located south, south-east and east of Mount Etna. As a result, measurements were not possible when the plume was drifted in other directions. The improvement of the FLAME network after 2010 helped to cover a bigger area, with stations all around the volcano. However, the plume is still sometimes at the spatial limit or outside of the scanner network, and measurements are not possible when there is a cloud cover above the volcano. Furthermore, we began the comparison after all the paroxysmal events occurred. Wind speed and plume height could have been better estimated if the project was known at that time.

The comparison was in good agreement only for April 10th, 2011 event, with both SO_2 flux and mass in the same range. Results of May 14th, 2008 highlight the importance of accurate wind speed data. The flux comparison shows a discrepancy between both sensors whereas the mass comparison, which does not require transport rate for its calculation, has a good agreement. Plume height is also important, as the November 16th, 2006 event shows it. Fluxes have the same trend but values with different magnitudes. After the emission, the plume is drifted away by winds of which speed and altitude may vary with time.

The plume transport direction is another important parameter to take into account as the geometry of the plume affects the flux calculation for the Mini-DOAS. The ground-based results of August 12th, 2011 eruption are likely underestimated because of a variation in the plume transport direction during the event.

Further research should be conducted with better wind speed and plume height measurements for paroxysmal events occurring in the morning. Those parameters and their variations with time and space should be better constrained and included in OMIplot to have more accurate results. More data are required to continue this comparison, make a validation of OMI volcanic SO_2 retrievals and improve the next generation of this kind of space-based sensors. Moreover, different techniques than the transects one should be used to estimate the flux with OMIplot in order to have several results which do not take into account the same parameters for the calculation, and especially wind speed and plume height. A better knowledge of SO_2 lifetime with the atmospheric conditions above Mount Etna would also permit to compare the eruptions that occur in the afternoon with more accuracy.

7. References

Allard P. 1997. Endogenous magma degassing and storage at Mount Etna. Geophysical Research Letters. 24:2219-2222.

Allard P, Burton M, Mure F. 2005. Spectroscopic evidence for a lava fountain driven by previously accumulated magmatic gas. Nature. 433:407-410.

Andronico D, Corsaro R A. 2011. Lava fountains during the episodic eruption of South–East Crater (Mt. Etna), 2000: insights into magma-gas dynamics within the shallow volcano plumbing system. Bulletin of Volcanology. 73:1165-1178.

Azzaro R, Barbano MS. 2000. Analysis of the seismicity of Southeastern Sicily: a proposed tectonic interpretation. Annali di Geofisica. 43:171-188.

Barberi F, Gasparini P, Innocenti F, Villari L. 1974. Volcanism of the southern Tyrrhenian Sea and its geodynamic implications. Journal of Geophysic Research. 78:5221-5232.

Berresheim H, Wine P, Davis D. 1995. Sulfur in the Atmosphere, in Composition Chemistry, and Climate of the Atmosphere, edited by H. B. Singh. p. 544, Wiley.

Bonaccorso A, Bonforte A, Calvari S, Del Negro C, Di Grazia G, Ganci G, Neri M, Vicari A, Boschi E. 2011a. The initial phases of the 2008–2009 Mount Etna eruption: A multidisciplinary approach for hazard assessment. Journal of Geophysic Research. 116, B03203.

Bonaccorso A, Caltabiano T, Currenti G, Del Negro C, Gambino S, Ganci G, Giammanco S, Greco F, Pistorio A, Salerno G, Spampinato S, Boschi E. 2011b. Dynamics of a lava fountain revealed by geophysical, geochemical and thermal satellite measurements: The case of the 10 April 2011 Mt Etna eruption. Geophysical Research Letters. 38, L24307.

Branca S, Del Carlo P. 2004. Eruptions of Mt Etna during the past 3,200 years: a revised compilation integrating the historical and stratigraphic records. In: Bonaccorso A, Calvari S, Coltelli M, Del Negro C, Falsaperla S (eds) Mount Etna volcano laboratory. AGU (Geophysical monograph series), vol 143:1-27.

Bruno N, Caltabiano T, Giammanco S, Romano R. 2001. Degassing of SO2 and CO2 at Mount Etna (Sicily) as an indicator of pre-eruptive ascent and shallow emplacement of magma. Journal of Volcanology and Geothermal Research. 110:137-153.

Burton M, Caltabiano T, Salerno GG, Mure F, Condarelli D. 2004. Automatic measurements of SO2 flux on Stromboli and Mt. Etna using a network of scanning UV spectrometers. Geophysical Research Abstracts. 6,03970.

Cadoux A, Blichert-Toft J, Pinti DL, Albarède F. 2007. A unique lower mantle source for southern Italy volcanic. Earth and Planetary Science Letters. 259:227-238.

Caltabiano T, Romano R, Budetta G. 1994. SO_2 flux measurements at Mount Etna. Journal of Geophysic Research. 99:12809-12819.

Calvari, S, Salerno GG, Spampinato L, Gouhier M, La Spina A, Pecora E, Harris AJL, Labazuy P, Biale E, Boschi E. 2011. An unloading foam model to constrain Etna's 11–13 January 2011 lava fountaining episode. Journal of Geophysic Research. 116, B11207.

Carn SA, Lopez TM. 2011a. Opportunistic validation of sulfur dioxide in the Sarychev Peak volcanic eruption cloud. Atmospheric Measurement Techniques. 4:1705-1712.

Carn SA. "OMIplot," https://vhub.org/resources/682, 2011b.

Casadevall TJ, Johnston DA, Harris DM, Rose WI, Malinconico LL, Stoiber RE, Bornhorst TJ, Williams SN, Woodruff L, Thompson JM. 1981. SO2 emission rates at Mount St. Helens from March 29 through December, 1980. In: P.W. Lipman and D.R. Mullineaux (Editors), The 1980 eruptions of Mount St. Helens, Washington. United States Geological Survey, Washington, D.C. 1-844.

Charlson RJ, Schwartz SE, Hales JM, Cess RD, Coakley JA, Hansen JE, Hofmann DJ. 1992. Climate Forcing by Anthropogenic Aerosols. Science. 255:423-430.

Chester DK, Duncan AM, Guest JE. 1987. The pyroclastic deposits of Mount Etna volcano, Sicily. Geological Journal. 22:225-243.

Ciuccarelli C. 2001. L'eruzione del 1669 e le modificazioni urbane di Catania. In: Boschi,E., Guidoboni, E. (Eds.), Catania terremoti e lave dal mondo antico alla fine del Novecento. Bologna. 94-104.

Ciuccarelli C. 2004. In margine all'attività dei vulcani italiani: storie di grandi disastri e pericolosi eventi minori: Giornale di Storia Contemporanea. In: Guidoboni, E. (Ed.), Storia ed Eventi Naturali Estremi in Italia: Strategie e Risultati di Ricerche Interdisciplianari. vol. 2 :51-68.

Clocchiatti R, Condomines M, Guénot N, Tanguy J-C. 2004. Magma changes at Mount Etna: The 2001 and 2002-2003 eruptions. Earth and Planetary Science Letters. 227:397-414.

Coltelli M, Del Carlo P, Vezzoli L. 1995. Stratigraphy of the Holocene Mt. Etna explosive eruptions. Periodico di Mineralogia Roma. 64:145-146.

Coltelli M, Del Carlo P, Vezzoli L. 1998. Discovery of a Plinian basaltic eruption of Roman age at Etna volcano, Italy. Geology. 26:1095-1098.

Coltelli M, Del Carlo P, Vezzoli L. 2000. Stratigraphic constraints for explosive activity in the past 100 ka at Etna Volcano, Italy. International Journal of Earth Sciences. 89:665-677.

Coltelli M, Garduño VH, Neri M, Pasquaré G, Pompilio M. 1994. Geology of the northern wall of Valle del Bove, Mt. Etna (Sicily). Acta Vulcanologica. 5:55-68.

Condomines M, Tanguy JC, Kieffer G, Allégre CJ. 1982. Magmatic evolution of a volcano studied by ^{230}Th–^{238}U disequilibrium and trace elements systematics: the Etna case. Geochimica e Cosmochimica Acta. 46:1397-1416.

Corsaro RA, Cristofolini R, Patane L. 1996. The 1669 eruption at Mount Etna: chronology, petrology and geochemistry, with inferences on the magma sources and ascent mechanisms. Bulletin of Volcanology. 58:348-358.

Corsaro RA, Cristofolini, R. 1997. Geology, geochemistry and mineral chemistry of tholeiitic to transitional Etnean magmas. Acta Vulcanologica. 9:55-66.

Duncan AM. 1976. Pyroclastic flow deposits in the Adrano area of Mount Etna, Sicily. Geological Magazine. 113:357-363.

Edmonds M, Herd RA, Galle B, Oppenheimer CM. 2003. Automated, high time-resolution measurements of SO2 flux at Soufrière Hills Volcano, Montserrat. Bulletin of Volcanology. 65:578-586.

Gillot PY, Kieffer G, Romano R. 1994. The evolution of Mount Etna in the light of potassium-argon dating. Acta Vulcanologica. 5:81-87.

Guest JE, Chester DK, Duncan AM. 1984. The Valle del Bove, Mount Etna: its origin and relation to the stratigraphy and structure of the volcano. Journal of Volcanology and Geothermal Research. 21:1-23.

Gvirtzman Z and Nur A. 1999. The formation of Mount Etna as the consequence of slab rollback. Nature. 401:782-785.

Hansell A and Oppenheimer C. 2004. Health hazards from volcanic gases: a systematic literature review. Archives of Environmental Health. 59:628-639.

INGV Sezione di Catania – Osservatorio Etneo [Internet]:
http://www.ct.ingv.it/index.php?option=com_docman&Itemid=344&lang=en

Jaeschke W, Berresheim H, Georgii HW. 1982. Sulfur emissions from Mount Etna. Journal of Geophysic Research. 87:7253-7261.

Katsouyanni K, Touloumi G, Spix C, Schwartz J, Balducci F, Medina S, Rossi G, Wojtyniak B, Sunyer J, Bacharova L, Schouten JP, Ponka A, Anderson HR. 1997. Short-term effects of ambient sulphur dioxide and particulate matter on mortality in 12 European cities: Results from time series data from the APHEA project. Air pollution and health: A European approach, BMJ(Clinical Research Ed.). 314:1658-1663.

Kieffer G. 1973. Une éruption à caractères katmaiens, à l'origine de coulées ponceuses et de coulées de ponces, responsable de la formation de la caldeira du Cratère Elliptique de l'Etna (Sicile). Comptes Rendus de l'Académie des Sciences de Paris. 277D :2321-2324.

Kieffer G. 1985. Evolution structurale et dynamique d'un grand volcan poligénique: stades d'édification et activité actuelle de l'Etna Sicile. Annales Scientifiques de l'Université de Clermont–Ferrand II, Géologie et Minéralogie. 84:497.

Krotkov NA, Carn SA, Krueger AJ, Bhartia PK, Yang K. 2006. Band residual difference algorithm for retrieval of SO2 from the Aura Ozone Monitoring Instrument (OMI). IEEE Transactions on Geoscience and Remote Sensing. 44:1259-1266.

Krueger AJ. 1983. Sighting of El Chichón Sulfur Dioxide Clouds with the Nimbus 7 Total Ozone Mapping Spectrometer. Science. 220:1377-1379.

Levelt PF, van den Oord GHJ, Dobber MR, Mälkki A, Visser H, de Vries J, Stammes P, Lundell J, Saari H. 2006. The Ozone Monitoring Instrument. IEEE Transactions on Geoscience and Remote Sensing. 44:1093-1101.

Likens GE, Bormann FH. 1974. Acid rain: A serious regional environmental problem. Science. 184:1176-1179.

Marone F, van der Lee S, Giardini D. 2004. Three-dimensional upper-mantle S-velocity model for the Eurasian-Africa plate boundary region. Geophysical Journal International. 158:109-130.

McGonigle AJS, Oppenheimer C, Hayes AR, Galle B, Edmonds M, Caltabiano T, Salerno G, Burton M. 2003. Volcanic sulphur dioxide fluxes from Etna, Vulcano and Stromboli measured with an automated scanning ultraviolet spectrometer. Journal of Geophysic Research. 108:B9.

Métrich N, Clocchiatti R. 1989. Melt inclusion investigation of the volatile behaviour in historic alkaline magmas of Etna. Bulletin of Volcanology. 51:185-198.

Métrich N, Clocchiatti R, Mosbah M, Chaussidon M. 1993. The 1989-1990 activity of Etna magma mingling and ascent of H20-CI-S-rich basaltic magma. Evidence from melt inclusions. Journal of Volcanology and Geothermal Research. 59:131-144.

Moffat AJ, Millán MM. 1971. The applications of optical correlation techniques to the remote sensing of SO2 plumes using sky light. Atmospheric Environment (1967) 5:677-690.

Montelli R, Nolet G, Dahlen FA, Masters G. 2006. A catalogue of deep mantle plumes: New results from finite frequency tomography. Geochemistry Geophysics Geosystems. 7:Q11007.

Newcomb G, Millán MM. 1970. Theory, applications and results of the long-line correlation spectrometer. IEEE Transactions on Geoscience Electronics. 8:149-157.

Noxon JF. 1975. Nitrogen dioxide in stratosphere and troposphere measured by ground-based absorption spectroscopy. Science. 189:547-549.

Rodgers C. 1976. Retrieval of atmospheric temperature and composition from remote measurements of thermal radiation. Reviews of Geophysics. 14:609-624.

Rodgers C. In: Taylor FW. 2000. (Ed.), Inverse methods for atmospheric sounding, theory and practice, series on atmospheric, oceanic and planetary physics – vol. 2.

Romano R, Guest JE. 1979. Volcanic geology of the summit and northern flank of Mount Etna, Sicily. Bollettino della Societa Geologica Italiana. 98:189-215.

Platt U. 1994. Differential Optical Absorption Spectroscopy (DOAS). In: Sigrist, M.W. (Ed.), Air Monitoring by Spectroscopy Techniques. Chemical analysis Series, vol.127.Wiley, New York, 27-84.

Platt U, Stutz J. 2008. Differential Optical Absorption Spectroscopy Principles and Applications, Series: Physics of Earth and Space Environments. Springer.

Salerno G, Burton M, Oppenheimer C, Caltabiano T, Tsanev VI, Bruno N. 2009a. Novel retrieval of volcanic SO2 abundance from ultraviolet spectra. Journal of Volcanology and Geothermal Research. 181:141-153.

Salerno G, Burton M, Oppenheimer C, Caltabiano T, Randazzo D, Bruno N, Longo V. 2009b. Three-years of SO2 flux measurements of Mt. Etna using an automated UV scanner array: Comparison with conventional traverses and uncertainties in flux retrieval. Journal of Volcanology and Geothermal Research. 183:76-83.

Scarfi L, Langer H, Scaltrito A. 2009. Seismicity, seismotectonics and crustal velocity structure of the Messina Strait (Italy). Physic of the Earth and Planete Interiors. 1777:65-78.

Schiano P, Clocchiatti R, Ottolini L, Busà T. 2001. Transition of Mount Etna lavas from a mantle-plume to an island arc magmatic source. Nature. 412:900-904.

Smithsonian/USGS – Global Volcanism Program [Internet]:
http://www.volcano.si.edu/world/volcano.cfm?vnum=0101-06=&volpage =weekly

Spilliaert N, Allard P, Métrich N, Sobolev AV. 2006. Melt inclusion record of the conditions of ascent, degassing, and extrusion of volatile-rich alkali basalt during the powerful 2002 flank eruption of Mount Etna (Italy). Journal of Geophysical Research. 111:B04203.

Spinei E, Carn SA, Krotkov NA, Mount GH, Yang K, Krueger AJ. 2010. Validation of ozone monitoring instrument SO2 measurements in the Okmok volcanic cloud over Pullman, WA, July 2008. Journal of Geophysical Research. 115:1-14.

Stevenson DS, Johnson CE, Collins WJ, Derwent RG. 2003. The tropospheric sulphur cycle and the role of volcanic SO2 In: C. Oppenheimer, D.M. Pyle and J. Barclay (Editors), Volcanic Degassing. Geological Society, Bath, UK. 295-305.

Stoiber RE, Jepsen A. 1973. Sulfur Dioxide Contributions to the Atmosphere by Volcanoes. Science. 182:577-578.

Stoiber RE, Malinconico LL, Williams SN. 1983. Use of the correlation spectrometer at volcanoes. In: Tazieff, H., Sabroux, J.C. (Eds.), Forecasting Volcanic Events. Elsevier, Amsterdam. 425-444.

Sutton AJ, Elias T, Gerlach TM, Stokes JB. 2001. Implications for eruptive processes as indicated by sulfur dioxide emission from Kīlauea volcano, Hawaii, 1979–1997. Journal of Volcanology and Geothermal Research. 108:283-302.

Tanguy J-C, Condomines M, Kieffer G. 1997. Evolution of the Mount Etna magma: Constraints on the present feeding system and eruptive mechanism. Journal of Volcanology and Geothermal Research. 75:221-250.

Ware JH, Ferris JrBG, Dockery DW, Spengler JD, Stram DO, Speizer FE. 1986. Effects of ambient sulfur oxides and suspended particles on respiratory health of preadolescent children. The American Review of Respiratory Disease. 5:834-842.

Watson IM, Oppenheimer C, Voight B, Francis PW, Clarke A, Stix J, Miller A, Pyle DM, Burton MR, Young SR, Norton G, Loughlin S, Darroux B. 2000. The relationship between degassing and ground deformation at Soufriere Hills Volcano, Montserrat. Journal of Volcanology and Geothermal Research. 98:117-126.

Yang K, Krotkov NA, Krueger AJ, Carn SA, Bhartia PK, Levelt PF. 2007. Retrieval of large volcanic SO2 columns from the Aura Ozone Monitoring Instrument: Comparison and limitations. Journal of Geophysical Research. 112:D24S43.

Yang K, Krotkov NA, Krueger AJ, Carn SA, Bhartia PK, Levelt PF. 2009. Improving retrieval of volcanic sulfur dioxide from BUV satellite observations. Geophysical Research Letters. 36:L03102.

Yang K, Liu X, Bhartia PK, Krotkov NA, Carn SA, Hughes EJ, Krueger AJ, Spurr RJD, Trahan SG. 2010. Direct retrieval of sulfur dioxide amount and altitude from spaceborne hyperspectral UV measurements: Theory and application. Journal of Geophysical Research. 115:D00L09.

Young S, Francis PW, Barclay J, Casadevall TJ, Gardner CA, Darroux B, Davies MA, Delmelle P, Norton GE, Maciejewski AJH, Oppenheimer C, Stix J,Watson IM. 1998. Monitoring SO2 emission at the Soufrière Hills volcano: implications for changes in eruptive conditions. Geophysical Research Letters. 25:3681.

8. Appendix

A: Copyright for Figure 2.2 (Personal communication through e-mail)

Giuseppe Salerno giuseppe.salerno@ct.ingv.it 23 avril

Dear Celine,

I know, it's not easy to find overlapped ground-satellite days, maybe just few case studies it's a good start, why the results retrieved from the compared days are not good?

Flame: right now the UV scanning network consists of nine scanners all stations have the same technology (attached fig). no problme, about the INGV map, state the appropiate reference (e.g., courtesy of Istituto Nazionale di Geofisica e Vulcanologia, Osservatorio Etneo, Italy)

If you have a skype account we can make a plan to have a chat, though it's not easy due to the time zone, anway we can try it.

all the best

Giuseppe

Istituto Nazionale di Geofisica e Vulcanologia, Osservatorio Etneo, Italy
Piazza Roma, 2 - 95123, Catania - Italy

office: +39 095 716 5829; mobile: +39 347 80 48788; fax: +39 095 716 5829
website: www.ingv.it; www.ct.ingv.it

B: Copyright for Figure 4.1 (Personal communication through e-mail)

céline mandon 15 aout

Hey Giuseppe,

As you noticed I used the GoogleEarth map with the FLAME stations location in my thesis.

The problem is that I would need GoogleEarth's permission to use it.

I found one of your map of the network in your paper: Three-years of SO2 flux measurements of Mt. Etna using an automated UV scanner array: Comparison with conventional traverses and uncertainties in flux retrieval. I added the 4 new stations on it.

I now need your permission to use it in my thesis.

I attach it so you can see the changes I made.

Hope you are enjoying your summer.

Celine

Giuseppe Salerno giuseppe.salerno@ct.ingv.it 16 aout

hello Celine, nice to hear from you,

the picture is fine, you got the permission.

Please remember that flame data has been provided just for the the thesis, since these data results from a team work any official report, article and/or presentation at conferences, should involve my team as co-author.

Please if you need other help do not hesitate to contact me

all the best

Giuseppe

C: Copyright for Figure 2.1 (Personal communication through e-mail)

céline mandon 15 aout

Hello,

I'm student at Michigan Technological University in the USA and I made my master's thesis on

SO2 fluxes at Mount Etna, in collaboration with Giuseppe Salerno from the INGV.

I would like to use in my thesis a figure from one of your paper: Seismicity, seismotectonics and crustal velocity structure of the Messina Strait (Italy), figure 1a, the simplified tectonic map.

I modified it a little bit but I still need your permission to publish it in my thesis.

Waiting for your answer,

Best regards.

Céline Mandon

Luciano Scarfì scarfi@ct.ingv.it 19 aout

Hello Céline,

I'm sorry for the late reply but I'm on holidays.
If you cite the source I have nothing against it.

Bye

Luciano Scarfì